### Title

Functional Reduction in Cannabinoid-Sensitive Heterotypic Inhibition of Dentate Basket Cells in Epilepsy: Impact on Network Rhythms




### Journal

Cerebral Cortex, 26(11)

### ISSN

1047-3211



### Authors

Yu, Jiandong
Proddutur, Archana
Swietek, Bogumila
et al.



### Publication Date

2016-10-01

### DOI

10.1093/cercor/bhv199

Peer reviewed

*Cerebral Cortex*, October 2016;26: 4299–4314

**doi:10.1093/cercor/bhv199**
Advance Access Publication Date: 22 September 2015
Original Article

ORIGINAL ARTICLE

# Functional Reduction in Cannabinoid-Sensitive Heterotypic Inhibition of Dentate Basket Cells in Epilepsy: Impact on Network Rhythms

Jiandong Yu[1,2], Archana Proddutur[2], Bogumila Swietek[2], Fatima S. Elgammal[2], and Vijayalakshmi Santhakumar[2]

[1]Center for Neuropsychiatric Diseases, Institute of Life Science, Nanchang University, Nanchang 330031, China, and [2]Department of Pharmacology, Physiology, and Neuroscience, Rutgers New Jersey Medical School, Newark, NJ 07103, USA

Address correspondence to Dr Vijayalakshmi Santhakumar, Department of Pharmacology, Physiology, and Neuroscience, Rutgers New Jersey Medical School, MSB-H-512, 185 S. Orange Ave. Newark, NJ 07103, USA. Email: santhavi@njms.rutgers.edu

## Abstract

Strong perisomatic inhibition by fast-spiking basket cells (FS-BCs) regulates dentate throughput. Homotypic FS-BC interconnections that support gamma oscillations, and heterotypic inputs from diverse groups of interneurons that receive extensive neurochemical regulation, together, shape FS-BC activity patterns. However, whether seizures precipitate functional changes in inhibitory networks and contribute to abnormal network activity in epilepsy is not known. In the first recordings from dentate interneuronal pairs in a model of temporal lobe epilepsy, we demonstrate that status epilepticus (SE) selectively compromises GABA release at synapses from dentate accommodating interneurons (AC-INs) to FS-BCs, while efficacy of homotypic FS-BC synapses is unaltered. The functional decrease in heterotypic cannabinoid receptor type 1 ($CB_1R$)-sensitive inhibition of FS-BCs resulted from enhanced baseline $GABA_B$-mediated suppression of synaptic release after SE. The frequency of $CB_1R$-sensitive inhibitory synaptic events in FS-BCs was depressed early after SE induction and remained reduced in epileptic rats. In biologically based simulations of heterogeneous inhibitory networks and excitatory–inhibitory cell networks, experimentally identified decrease in reliability of AC-IN to FS-BCs synaptic release reduced theta power and theta-gamma coupling and enhanced gamma coherence. Thus, the experimentally identified functional reduction in heterotypic inhibition of FS-BCs can contribute to compromised network oscillations in epilepsy and could precipitate memory and cognitive co-morbidities.

**Key words:** cannabinoid, dentate gyrus, epilepsy, interneuron, oscillations

## Introduction

Epilepsy, a disorder of enhanced network excitability and synchrony, is associated with altered inhibitory function. In the dentate gyrus, GABAergic fast-spiking basket cells (FS-BCs), which express parvalbumin (PV) and underlie granule cell perisomatic inhibition (Kraushaar and Jonas 2000; Bartos et al. 2002), are central to regulating network excitability and throughput. Dentate FS-BCs are highly interconnected through GABAergic and electrical synapses (Bartos et al. 2001). The reliable, strong, and fast synaptic interconnections between FS-BC are important for generating gamma (40–100 Hz) frequency oscillations (Bartos et al. 2002) which provide a temporal framework for memory encoding. Epilepsy is associated with alterations in network oscillations and often presents with memory dysfunction (Bragin et al. 2005; Chauviere et al. 2009; Rattka et al. 2013), suggesting that FS-BC networks may be compromised. Experimental studies have demonstrated that status epilepticus (SE) modifies FS-BC physiology, decreasing excitatory drive to FS-BCs, enhancing

 

FS-BC extrasynaptic inhibition and depolarizing FS-BC GABA reversal (Zhang and Buckmaster 2009; Yu et al. 2013). Additionally, reliability and potency of FS-BC synapses to granule cells are compromised in epilepsy (Zhang and Buckmaster 2009). In computational studies, changes in FS-BC tonic inhibition, synaptic characteristics, and addition of inputs from nonfast-spiking interneurons to FS-BC networks have been shown to impact oscillatory dynamics (White et al. 2000; Bartos et al. 2001; Wulff et al. 2009; Proddutur et al. 2013; Yu et al. 2013). Given the role of interneuronal inhibition in structuring network behavior and oscillations (Buzsáki 2006; Klausberger and Somogyi 2008; Chamberland and Topolnik 2012), it is important to determine whether the characteristics of synaptic connections to FS-BCs are altered after SE. Delineating the changes in interneuronal connectional features in epilepsy will provide essential mechanistic insights into the alterations in network oscillations, the generation of hypersynchrony, and behavioral co-morbidities in epilepsy.

While the fast-spiking phenotype and high-temporal fidelity of perisomatic synapses enable FS-BCs to mediate precise and robust inhibition, they have a limited repertoire of direct modulatory inputs (Armstrong and Soltesz 2012). Thus, contextual modulation of FS-BC activity depends on their diverse heterotypic inhibitory inputs (Savanthrapadian et al. 2014). Granule cells and interneurons alike receive excitatory drive in the theta frequency range (4–12 Hz) and generate gamma oscillations driven by local interneuronal networks (Pernia-Andrade and Jonas 2014). Theta-gamma oscillations, which are particularly robust in the dentate gyrus (Bragin et al. 1995), serve as reference signals for memory encoding/retrieval and are altered in epilepsy (Fell et al. 2001; Worrell et al. 2004; Bragin et al. 2005; Jutras et al. 2009). In hippocampal network simulations, heterotypic inhibition of FS-BCs from neurons with adapting firing pattern, membrane sag, and slow synaptic kinetics are necessary for the generation of robust theta rhythm in networks with gamma oscillations (White et al. 2000; Rotstein et al. 2005). In the dentate, accommodating interneurons (AC-INs) showing adapting firing pattern and membrane sag include hilar commissural–associational pathway (HICAP)-associated cells which express cholecystokinin (CCK) and physiologically similar total molecular layer (TML) cells (Han et al. 1993; Mott et al. 1997; Hosp et al. 2014; Yu et al. 2015). Both HICAP and TML cells have molecular layer dendrites (Mott et al. 1997; Hosp et al. 2014) and are ideally located to receive and reinforce entorhinal theta-modulated inputs to FS-BCs. Additionally, CCK-positive interneurons receive diverse neuromodulatory inputs (Freund 2003; Armstrong and Soltesz 2012) which, by way of heterotypic inputs to FS-BCs, can regulate FS-BC-generated network rhythms. In order to determine whether epilepsy results in a fundamentally altered inhibitory network that could contribute to dynamic changes in network rhythms and synchrony, we examined whether homotypic and heterotypic inhibition of FS-BCs is altered after pilocarpine-induced SE.

## Materials and Methods

### Animals

All experiments were performed in accordance with Rutgers-NJMS, Newark, NJ, IACUC. Postnatal days 25–27, male, Wistar rats were pretreated with scopolamine (1 mg/kg, s.c.) followed by pilocarpine (300 mg/kg, i.p.) to induce 60 min of Racine stage 3 or greater seizures followed by diazepam (10 mg/kg, i.p.) to terminate SE (Yu et al. 2013). Controls received saline followed by diazepam after 2 h (Yu et al. 2013). A subset of single-cell recordings in Figure 1 were conducted in 30- to 35-day-old naïve rats. A group of experimental rats were implanted with cortical screw electrodes (Pinnacle Technology) 19–35 days after SE. Following a 5- to 10-day recovery, animals underwent video-EEG monitoring (Pinnacle Technology) for 12 h/day for 3 days. Data were sampled at 1 kHz and acquired using Powerlab 16/35. Since 11 of 12 (91.67%) rats recorded between 25 and 45 days post-SE used in this study showed spontaneous electrographic seizures (defined as high-amplitude activity, with a magnitude at least 2 times the standard deviation of the baseline) accompanied by simultaneous behavioral seizures (defined as ≥Racine stage 3), post-SE rats >40 days were deemed epileptic.

### Physiology

Rats were euthanized under isoflurane anesthesia 1 week (6–8 days) or 40–70 days after SE or saline treatment. Horizontal brain slices (300 μM) were cut in ice-cold oxygenated sucrose artificial cerebrospinal fluid (sucrose-aCSF) incubated at 32 ± 1 °C for 30 min in a chamber containing 50% sucrose-aCSF and 50% aCSF and held at room temperature (Yu et al. 2013). Hilar-granule cell layer-border interneurons were patched at 33 ± 1°C under infrared differential interference contrast using a Nikon FN-1 microscope (×40 water objective). Recording electrodes (3–4 MΩ) contained (in mM) 70 KCl, 70 K-gluconate, 10 4-(2-hydroxyethyl)-1-piperazineethanesulfonic acid, 2 $MgCl_2$, 0.2 ethylene glycol tetraacetic acid, 2 sodium Adenosine 5′-triphosphate, 0.5 sodium Guanosine 5′-triphosphate, 10 phosphocreatine, and 0.2% biocytin. Intrinsic properties were determined from responses to 1.5-s current injections from a –70-mV holding potential. Neurons with adapting firing without stuttering, and input resistance over 150 MΩ were considered AC-INs. FS-BCs showed nonadapting, high-frequency firing, and low input resistance (<150 MΩ). Post hoc biocytin immunostaining and morphological analysis were used to definitively identify AC-INs based on dendrites in the hilus and molecular layer and axonal projections either in the inner molecular layer (HICAP) or spanning the molecular layer (TML) (Zhang and Buckmaster 2009; Hosp et al. 2014). FS-BCs had axon terminals in the granule cell layer (Hefft and Jonas 2005; Yu et al. 2013). Both pre- and postsynaptic cells were identified based on physiological characteristics followed by post hoc confirmation based on either morphological or neurochemical identity or both. Neurons with spiny dendrites confined to the hilus-presumed to be hilar-perforant pathway (HIPP)-associated cells and mossy cells were not analyzed. Unconnected neuron pairs in connection probability estimates were defined based on physiology.

Whole-cell voltage- and current-clamp recordings were obtained using Axon Instruments MultiClamp 700B (Molecular Devices, Sunnyvale, CA, USA). Signals were low-pass filtered at 3 kHz and digitized at 10 kHz and acquired using pCLAMP (Molecular Devices). For paired recordings, presynaptic interneurons were stimulated with 2–8 current pulses (3 ms, 700–1100 pA at 50 Hz) every 10 s in current-clamp mode while postsynaptic neurons were voltage-clamped at –70 mV. Only pairs showing stable recordings during repeated sweeps were used to analyze synaptic parameters. For spontaneous and miniature IPSC recordings, FS-BCs were held at –70 mV and recorded in glutamate receptor antagonist (3 mM kynurenic acid). Miniature inhibitory postsynaptic currents (mIPSCs) were recorded in 1 μm tetrodotoxin (TTX). Recordings were discontinued if series resistance increased by >20%. All salts and kynurenic acid were obtained from Sigma and SCH50911, (RS)-baclofen, WIN 55212-2, and

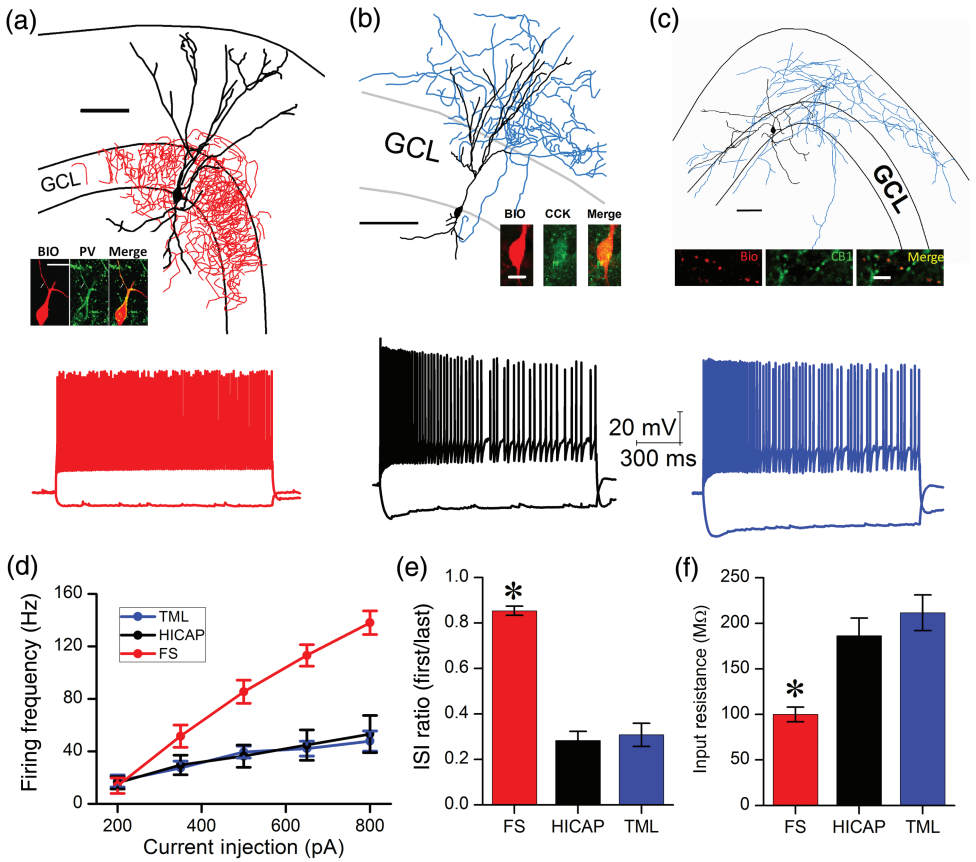


**Figure 1.** Physiological differences between FS-BC and AC-INs. (*a*) Morphological reconstruction of a fast-spiking basket cell (FS) above illustrates the dense axonal distribution (in red) in the granule cell layer. Fast nonadapting firing pattern of the FS-BC is shown below (in red). Insets show immunostaining of the soma and dendrite (arrow) for biocytin (right), parvalbumin (middle), and merged image (left). (*b*) Reconstruction of a CCK-expressing HICAP cell shows axonal distribution in the inner molecular layer. Insets show immunostaining of the soma for biocytin (right), CCK (middle), and merged image (left). The adapting firing during +500 pA current injection and hyperpolarizing response with membrane potential sag during −100 pA current injection are shown below. Note the difference in scale bar in the morphological reconstruction in *b*. Only GCL and inner third of the molecular layer are illustrated. (*c*) Reconstruction of a TML cell shows axonal distribution throughout the extent of the molecular layer. Insets of an axonal segment in the middle molecular layer show immunostaining for biocytin (right), $CB_1R$ (middle), and merged image (left). The adapting firing in response to a +500 pA current injection and hyperpolarizing response with sag during a −100 pA current injection are shown below. Scale bar, 100 µm for neuronal reconstructions and 25 µm for insets. GCL, granule cell layer. (*d*) Firing frequency of FS-BCs, HCAP, and TML cells in response to systematic increase in current injection. (*e*,*f*) Summary plots of interspike interval (ISI) ratio, measured as a ratio of the first and last ISI during a +500 pA current injection for 1500 ms (*e*) and input resistance (*f*) *$P < 0.05$, *t*-test compared with TML cell and HICAP cell.

AM251 were obtained from Tocris Bioscience. WIN 55212-2 and AM251 stock solutions were made in dimethylsulfoxide (DMSO) and diluted to a final DMSO concentration <0.1%.

## Anatomy

Recorded slices were fixed in 4% paraformaldehyde. Thick slices (300 µm) were incubated overnight with anti-PV antibody (PV-28, 1.5:1000, polyclonal rabbit, Swant) or anti-cannabinoid receptor type 1 ($CB_1R$) antibody (1:1000, polyclonal guinea pig, Frontier Science, Japan) in 0.3% Triton X-100 and 3% normal goat serum. Immunoreactions were revealed using Alexa 488-conjugated secondary antibodies. Biocytin was revealed using Alexa 594-conjugated streptavidin (1:1000). Sections were visualized and imaged using a Zeiss LSM510 confocal microscope (0.5 NA, ×20 objective). Cell reconstructions and morphological analyses were performed with Neurolucida V.10.02 (MBF Bioscience, Williston, VT, USA) using confocal image stacks (Yu et al. 2013).

A group of rats and age-matched controls were perfused 1 week or >40 days after SE. Sections were immunolabeled using monoclonal-mouse anti-PV (1.5:1000; Swant) or mouse anti-gastrin/CCK (1:3000, Cure, UCLA) and appropriate secondary antibodies (Yu et al. 2013). Controls in which primary antibody was omitted were routinely included. Sections were imaged using Nikon A1R confocal microscope with ×60 water objective. Cell counts were performed with the optical fractionator of Stereo Investigator V.10.02 (MBF Bioscience, Williston, VT, USA) on an Olympus BX51 microscope with a ×100 oil objective. In each section, the region of interest (ROI) including the granule cell layer and 100 µm of the subgranular hilus was outlined with a ×10 objective (Supplementary Fig. 5*a*). Sampling parameters were set at 100×: counting frame = 100 µm by 60 µm, dissector height =30 µm, and top guard zone=1 µm. An observer blind to control and post-SE groups marked the PV- or CCK-positive somata in the ROI. Approximately 25 sites per contour were selected for counting with randomized systematic sampling protocols in Stereo Investigator (Yu et al. 2013).

## Computational Modeling

FS-BC model was identical to Proddutur et al. (2013). A previously published multicompartmental hilar interneuron model (Santhakumar et al. 2005; Dyhrfjeld-Johnsen et al. 2007) was modified to generate the model AC-IN (Supplementary Fig. 6*b* and Tables 1 and 2). The heterogeneous interneuronal network

model including 200 FS-BCs and 200 AC-INs was implemented using NEURON 7.2 (Hines and Carnevale 1997). Homotypic neurons were connected in concentric rings with 15% connectivity among 70 local neurons. AC-IN to FS-BC connections were set to 15% among 70 local neurons. Synaptic conductance ($g_{Syn}$), rise, and decay times of FS-BC→FS-BC synapses ($g_{Syn}$: 7.6 nS, rise: 0.16 ms, and decay: 1.8 ms based on Bartos et al. 2002; Proddutur et al. 2013), AC-IN→FS-BC ($g_{Syn:}$ 5 nS, rise: 0.45 ms, and decay: 2.77 ms based on experimental data), and AC-IN→AC-IN ($g_{Syn}$: 4 nS, rise: 0.55 ms, and decay: 3.54 ms based on unpublished observations) were implemented using the Exp2Syn synaptic mechanism in NEURON. Changes in synaptic release probability (P) were implemented by modifying Exp2Syn to include independent probabilistic release for each synaptic connection. Occurrence of release at the synapse was based on thresholding at P of a uniform random number between 0 and 1. The release probability was $P_{FS\text{-}BC\rightarrow FS\text{-}BC} = 0.8$, $P_{AC\text{-}IN\rightarrow FS\text{-}BC} = 0.8$, and $P_{AC\text{-}IN\rightarrow AC\text{-}IN} = 0.3$ in "control networks" and $P_{FS\text{-}BC\rightarrow FS\text{-}BC} = 0.8$, $P_{AC\text{-}IN\rightarrow FS\text{-}BC} = 0.3$, $P_{AC\text{-}IN\rightarrow AC\text{-}IN} = 0.3$ in "Post-SE networks." All neurons were driven by sinusoidal current injections ($I_{inj\text{-}\theta}$) at 4–12 Hz, with a peak amplitude of 50 pA overriding a mean current injection of 200 pA in AC-INs and 500 pA in FS-BCs. Heterogeneity in cell firing was introduced by deriving the mean current injection for each cell from a Gaussian distribution amplitudes with 0.5% heterogeneity (%heterogeneity was defined as variance/mean × 100, Proddutur et al. 2013). Additionally, the start of current injection in each neuron had a random delay drawn from a Gaussian distribution (from values between 0 and 30% of the period of $I_{inj\text{-}\theta}$). FS-BC coherence was evaluated between 500 and 1500 ms using custom MATLAB code (Proddutur et al. 2013). Membrane potentials from 10 local FS-BCs between 500 and 1500 ms were sampled at 10 kHz and averaged to generate FS-BC-derived local field potential (LFP) traces used to evaluate frequency-power spectra and cross-frequency coupling. MATLAB code (provided by Dr. Adriano Tort, UFRN, Brazil) was used to calculate an entropy-based cross-frequency modulation index (MI) between theta (2–12 Hz) phase and gamma (30–100 Hz) amplitude as detailed previously (Tort et al. 2010).

Excitatory–inhibitory cell (E-I) networks included 1000 model granule cells (GCs) (Santhakumar et al. 2005) along with 200 FS-BCs and 200 AC-INs. In addition to the synaptic connections in the interneuron-only networks above, each FS-BC and AC-IN received synaptic inputs from 10 GCs. Synaptic parameters at GC→FS-BC and FS-BC→GC were as reported in earlier dentate models (Santhakumar et al. 2005; Dyhrfjeld-Johnsen et al. 2007; Yu et al. 2013). Synaptic parameters at GC→AC-IN and AC-IN→GC were constrained by parameters from hilar interneurons in our earlier network model (Yu et al. 2013). All neurons were driven by $I_{inj\text{-}\theta}$ at 4–12 Hz, with peak amplitude of 50 pA overriding a mean current injection of 200 pA in GCs and AC-INs and 500 pA in FS-BCs. Membrane potentials from 50 local GCs, sampled at 10 kHz, were averaged to generate GC-derived LFP for power spectral analysis.

### Analysis

Spontaneous inhibitory postsynaptic currents (sIPSCs) and mIPSCs were analyzed using Clampfit (Molecular Devices). Evoked IPSCs were measured using cursors. The "average" unitary inhibitory postsynaptic current (uIPSC) amplitude was calculated by averaging over all synaptic events including both synaptic failures and successful events while uIPSC "amplitude potency" was the calculated as the average amplitude of successful synaptic events excluding failures. The latencies of uIPSCs were measured from peak of presynaptic action potentials to onset of IPSCs. Cumulative probability plots of sIPSC parameters were constructed by pooling an equal number of sIPSCs from each cell and compared using Kolmogorov–Smirnov (K-S) test (SigmaPlot 12.3). Paired and unpaired Student's *t*-test, two-way repeated-measures ANOVA (TW-RM-ANOVA, SigmaPlot 12.3) and $\chi^2$ test were used to compare data, as appropriate. Data not conforming to a normal distribution were compared using Mann–Whitney *U*-test (*U*-test) (SigmaPlot 12.3, San Jose, CA, USA). Significance was set to $P < 0.05$. Data are reported as mean ± standard error of the mean or median and interquartile range (IQR), as appropriate.

## Results

### Homotypic FS-BC Synapse Characteristics Remain Unchanged After SE

Large pyramidal-shape neurons in the dentate hilar-granule cell border were physiologically classified as FS-BCs or AC-INs based on intrinsic properties. As illustrated in Figure 1, FS-BCs demonstrated significantly higher firing frequency (85.4 ± 8.8 Hz in response to +500 pA current injection, $n$=12 cells and >100 Hz during an 800-pA current injection), lower input resistance ($R_{in}$, 100.0 ± 8.0 MΩ, $n = 12$ cells), minimal spike frequency adaptation (interspike interval (ISI) ratio between first and last 2 spikes, $ISI_{first/last}$ ratio: 0.85 ± 0.02, $n = 12$) compared with both TML and HICAP cells. Additionally, FS-BCs lacked membrane sag during hyperpolarization (Fig. 1*a*). On post hoc morphological analysis, FS-BCs showed axonal arbors in the granule cell layer and expressed PV (Fig. 1*a*) as reported in earlier studies (Hefft and Jonas 2005; Yu et al. 2013). Consistent with the distribution of chandelier (axo-axonic) cells in the inner molecular layer of the dentate gyrus (Soriano et al. 1990), fast-spiking neurons recorded in the dentate hilar-granule cell border did not include neurons with axons exhibiting vertical aggregations of axonal varicosities or cartridges characteristic of axo-axonic cells. Thus, the fast-spiking neurons in this study were PV-expressing basket cells.

AC-INs included hilar neurons with hilar and molecular layer dendrites, and axons either predominantly in the inner molecular layer (CCK-expressing HICAP cells, Fig. 1*b*) or in all 3 molecular layers (TML cells, Fig 1c). TML cells express $CB_1R$ in their axon terminals (Fig. 1c, inset; Yu et al. 2015). However, unlike CCK-expressing HICAP cells, TML cells do not label for CCK (Yu et al. 2015). Comparison of the basic firing characteristics of morphologically identified HICAP and TML neurons did not reveal significant differences (Fig. 1*d*,*e*, frequency in Hz at 500 pA current injection, HICAP: 36.4 ± 8.5; TML: 39.5 ± 4.5, $P > 0.05$ by *t*-test; $ISI_{first/last}$ ratio, HICAP: 0.28 ± 0.04; TML: 0.31 ± 0.05, $P > 0.05$ by *t*-test $n = 10$ HICAP and 12 TML cells from control and naïve rats). Similarly, passive membrane properties were not different between HICAP and TML cells (Fig. 1*f*, $R_{in}$ in MΩ, HICAP: 186.5 ± 19.2; TML: 211.6 ± 19.6, $P > 0.05$ by *t*-test; resting membrane potential in mV, HICAP: −67.3 ± 3.0; TML: −63.4 ± 2.8, $P > 0.05$ by *t*-test; Sag ratio: HICAP: 0.80 ± 0.04; TML: 0.82 ± 0.02, $P > 0.05$ by *t*-test $n$ = 10 HICAP and 12 TML cells). Therefore, HICAP and TML cells were grouped together as AC-INs for further analysis. Neurons that showed fusiform or multipolar somata and those with spiny dendrites restricted to the hilus were presumed to be either HIPP or mossy cells and were excluded from analysis. Single cells and neurons in connected pairs were classified using physiological criteria and verified based on morphology and immunostaining.

We examined whether the basic physiological characteristics used for cell identification were altered in rats 1 week after pilocarpine-SE. FS-BCs from post-SE rats showed no difference

in average firing frequency in response to a 800-pA current injection (frequency in Hz, control: 138.0 ± 9.5, $n = 12$ cells, post-SE: 136.8 ± 12.7, $n = 11$ cells, $P = 0.94$ by $t$-test) and input resistance ($R_{in}$ in MΩ, control: 100.0 ± 8.0, $n = 12$ cells, Post-SE: 97.7 ± 9.0, $n = 11$ cells, $P = 0.84$ by $t$-test) from age-matched controls (data not shown). Similarly, the average firing frequency of AC-INs in response to a 800-pA current injection (frequency in Hz, control: 63.8 ± 6.1, $n = 25$ cells, post-SE: 64.8 ± 9.9, $n = 12$ cells, $P > 0.05$ by $t$-test) and input resistance ($R_{in}$ in MΩ, control: 236.9 ± 7.9, $n = 25$ cells, post-SE: 218 ± 11.6, $n = 12$ cells, $P > 0.05$ by $t$-test) were not different from controls (data not shown). In addition to the firing frequency and input resistance, resting membrane potential and spike frequency adaptation in FS-BCs and AC-INs were not altered in post-SE or epileptic rats (data not shown). Thus, the physiological characteristics used to identify FS-BCs and AC-INs remained unaltered in after SE.

To assess SE-induced changes in FS-BC synaptic inhibition, we recorded sIPSCs and mIPSCs. As illustrated in the schematic (Fig. 1*a*, upper panel) FS-BCs receive inhibitory inputs from several GABAergic neurons and can be identified based on their morphology, labeling for PV (Fig. 1*a*, middle panel) and nonadapting firing (Fig. 1*a*, lower panel). FS-BC sIPSC frequency and amplitude were significantly reduced in rats 1 week after SE (Fig. 2*b–d*; frequency in Hz, control: $\text{median}_{(IQR)} = 5.63_{(2.68–11.95)}$, $n = 20$ neurons; post-SE: $\text{median}_{(IQR)} = 4.68_{(2.23–10.28)}$, $n = 15$ neurons, $P < 0.05$, K-S test; amplitude in pA, control: $\text{median}_{(IQR)} = 20.77_{(11.75–36.09)}$, $n = 20$ neurons; post-SE: $\text{median}_{(IQR)} = 15.65_{(9.12–28.61)}$, $n = 15$ neurons, $P < 0.05$, K-S test), as shown previously (Yu et al. 2013). Frequency of FS-BC mIPSCs (in 1-μm TTX) was also reduced after SE (Fig. 2*e*,*f*, in Hz, control: $\text{median}_{(IQR)} = 4.75_{(2.04–12.05)}$, $n = 10$ neurons; post-SE: $\text{median}_{(IQR)} = 2.68_{(1.05–6.69)}$, $n = 9$ neurons, $P < 0.05$, K-S test), as has been observed in GCs (Kobayashi and Buckmaster 2003). However,

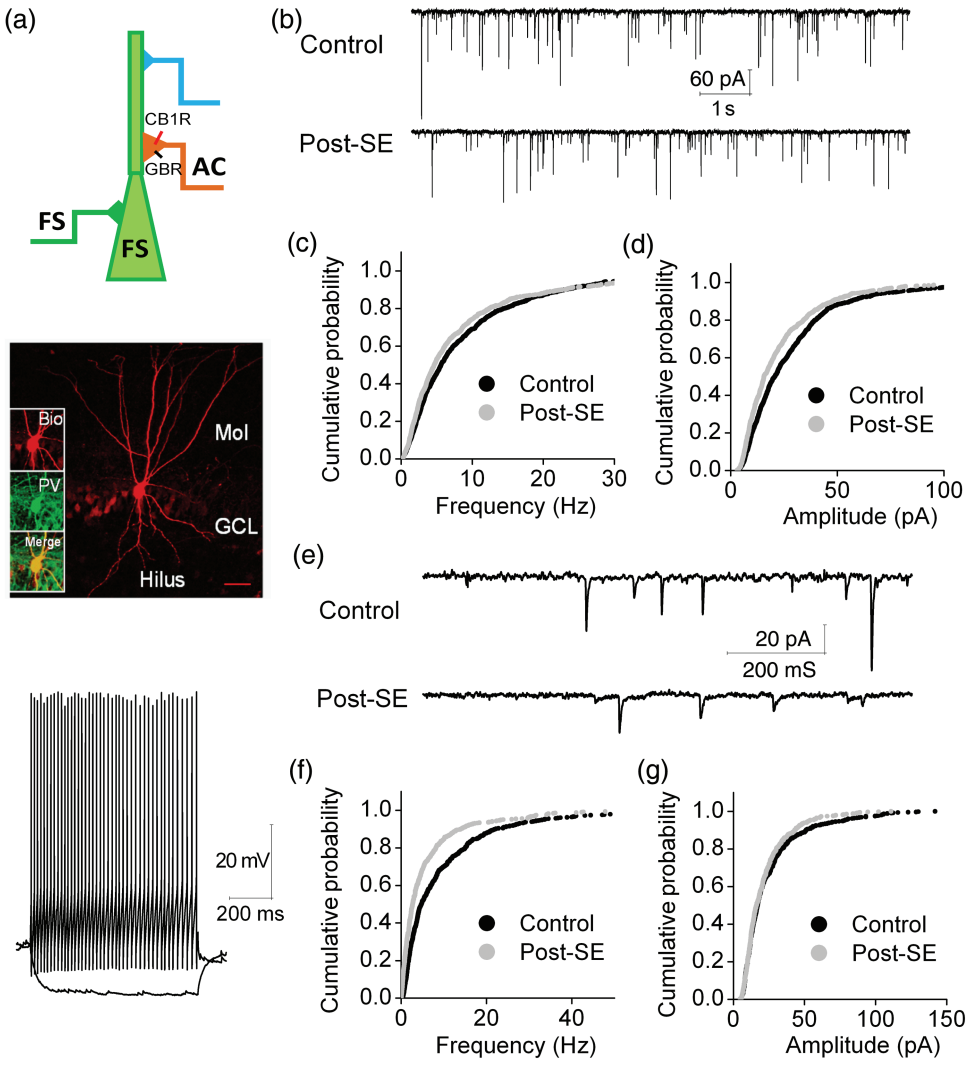


**Figure 2.** Status epilepticus compromises FS-BC synaptic inhibition. (*a*) Schematic of FS-BC inputs under whole-cell recording condition (top) illustrates potential inhibitory inputs from FS-BCs (FS in green), AC-INs (AC, in orange), and other interneurons (in blue). Presence of $GABA_BR$ (GBR) and cannabinoid receptor type 1 ($CB_1R$) on the AC-IN presynaptic terminal are illustrated. The middle panel shows maximum intensity projection of confocal image stacks of a FS-BC filled with biocytin (red) during recordings and labeled for PV (green). Insets: Confocal image of biocytin-filled soma (top inset in red) and labeling for PV (middle inset in green). Merged image (bottom inset) shows PV and biocytin co-labeling in the soma. Scale bar, 50 μm. Membrane voltage traces from the FS-BC (lower panel) illustrates the fast-spiking, nonadapting firing pattern during a +500 pA current injection and low membrane hyperpolarization in response to a −50 pA current injection. (*b*) Representative traces of spontaneous inhibitory synaptic currents (sIPSCs) from control (upper trace) and post-SE FS-BCs (lower trace). (*c*,*d*) Cumulative probability plots of sIPSC instantaneous frequency (*c*, $P < 0.05$, K-S test) and amplitude (*d*). (*e*) Representative traces of miniature IPSCs (mIPSCs) from control (upper trace) and post-SE FS-BCs (lower trace). (*f*,*g*) Cumulative probability plots of mIPSC instantaneous frequency (*f*) and amplitude (*g*).

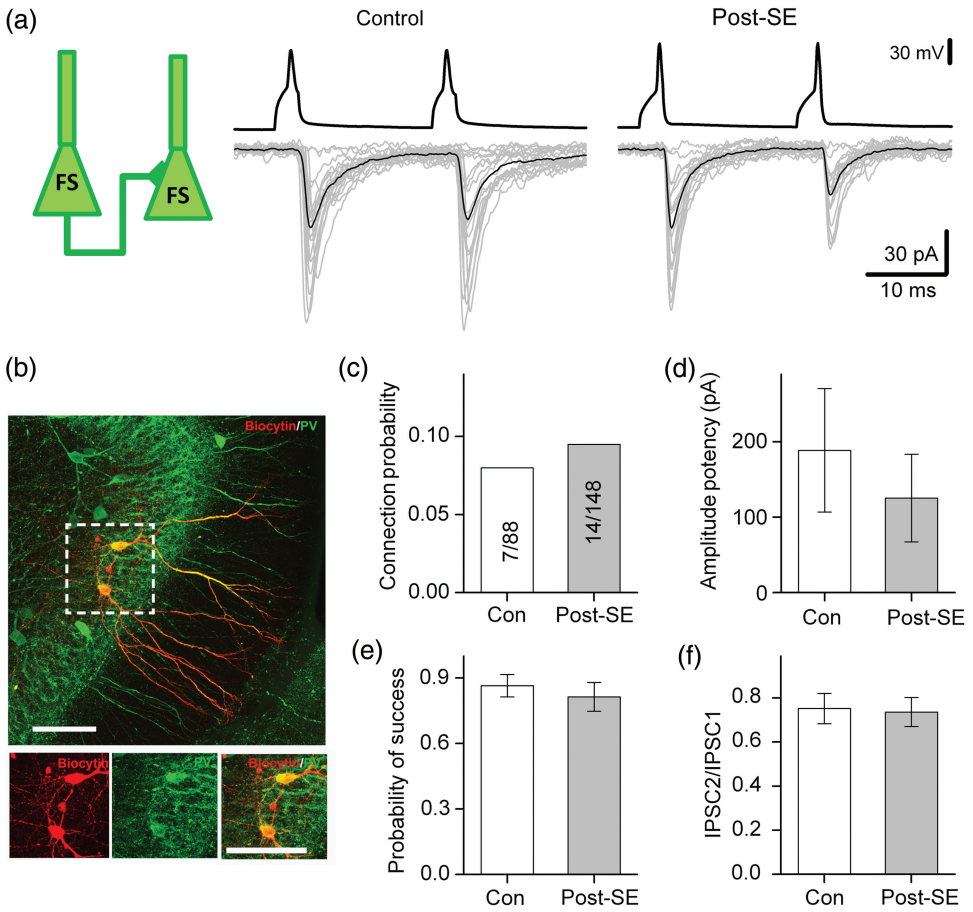


**Figure 3.** Unitary GABAergic synapses between FS-BCs are not modified after SE. (*a*) Schematic (left panel) illustrates the paired FS-BC (FS) recording condition. Example voltage traces above from presynaptic FS-BCs show a pair of action potentials (50 Hz). Current traces below show unitary IPSCs (30 individual sweeps in gray and averaged traces in black) in the synaptically connected FS-BC from control (middle panel) and post-SE (right panel) rats. (*b*) Confocal image of a pair of synaptically connected FS-BCs filled with biocytin (red) during recordings and labeled for PV (green). Insets: Confocal images of biocytin-filled somata (left) showing labeling for PV (middle) and merged image (right). Scale bar, 50 µm. (*c–f*) Summary plots of the connection probability (*c*), amplitude potency (*d*), probability of success (*e*), and paired pulse ratio at 50 Hz (*f*) in control and post-SE FS-BC pairs.

FS-BC mIPSC amplitude remained unchanged after SE (Fig. 2*g*: in pA, control: $\text{median}_{(\text{IQR})} = 17.01_{(11.15–29.5)}$, $n = 10$ neurons; post-SE: $\text{median}_{(\text{IQR})} = 16.22_{(10.92–26.88)}$, $n = 9$ neurons, $P > 0.05$, K-S test). Structural changes such as the loss of dentate interneurons, including somatostatin-expressing cells, and axon terminals after SE (Kobayashi and Buckmaster 2003; Sun et al. 2014), likely contribute to the early reduction in FS-BC synaptic inhibition. However, whether functional changes in the large amplitude, presumed perisomatic, and proximal dendritic synapses contribute to deficits in FS-BCs synaptic inhibition after SE is not known.

FS-BCs are typified by large amplitude, fast, and reliable synapses (Bartos et al. 2001, 2002). We examined whether post-SE changes in FS-BC interconnections underlie the changes in FS-BC synaptic inhibition. In FS-BC pairs (Fig. 3*a*,*b*), the probability of synaptic connections was not significantly altered after SE (Fig. 3*c*, control: 8%, 7/88 pairs, post-SE: 9.5%, 14/148 pairs, $P = 0.69$, $\chi^2$ test). The characteristic large unitary IPSC amplitude between FS-BC pairs (Bartos et al. 2001; Savanthrapadian et al. 2014) also failed to show a statistically significant difference after SE (Fig. 3*d*: amplitude potency excluding failures in pA, control: 188.8 ± 81.9, $n = 7$ pairs; post-SE: 125.5 ± 58.2, $n = 11$ pairs $P = 0.65$, *U*-test, average uIPSC amplitude including failures in pA, control: 185.6 ± 98.8, $n = 7$ pairs; post-SE: 119.1 ± 59.13, $n = 11$ pairs $P = 0.58$ by *U*-test). Similarly, the decay kinetics of FS-BC synapses was not altered after SE (weighted decay time constant in ms, control: 2.89 ± 0.43, $n = 7$ pairs; post-SE: 2.91 ± 0.20, $n = 11$ pairs $P = 0.95$, *U*-test). Crucially, homotypic FS-BC synapses maintained their characteristic high reliability after SE (Fig. 3*e*: probability of success, control: 0.86 ± 0.05, $n = 7$ pairs; post-SE 0.81 ± 0.07, $n = 11$ pairs, $P = 0.89$, *U*-test). Consistent with their high reliability, FS-BC uIPSCs showed paired- and multipulse depression which was not altered after SE (Fig. 3*a*,*f*, Supplementary Fig. 1*a*,*b*: paired pulse ratio, control: 0.75 ± 0.07, $n = 7$ pairs; post-SE: 0.74 ± 0.07, $n = 11$ pairs, $P = 0.87$, *t*-test). Stereological quantification of PV-labeled neurons in sections from rats perfused 1 week after SE or saline treatment revealed no post-SE reduction in the number of PV-expressing neurons in the hilar-granule cell layer border (number of cells in ROI per section, control: 38.35 ± 5.2; post-SE: 40 ± 8.5, $n = 18$ sections from 3 rats each, $P > 0.05$, *t*-test, data not shown). Together, our data show a lack of PV neuronal loss or significant differences in FS-BC connectional parameters in post-SE rats indicating that FS-BC networks are maintained after SE.

## Reduction in AC-IN Inhibition of FS-BCs After SE

Since homotypic inhibition of FS-BCs appears unchanged, we examined if heterotypic AC-IN inputs to FS-BCs are altered after SE. FS-BCs received synaptic inputs from AC-INs (Fig. 4*a*,*b*). The

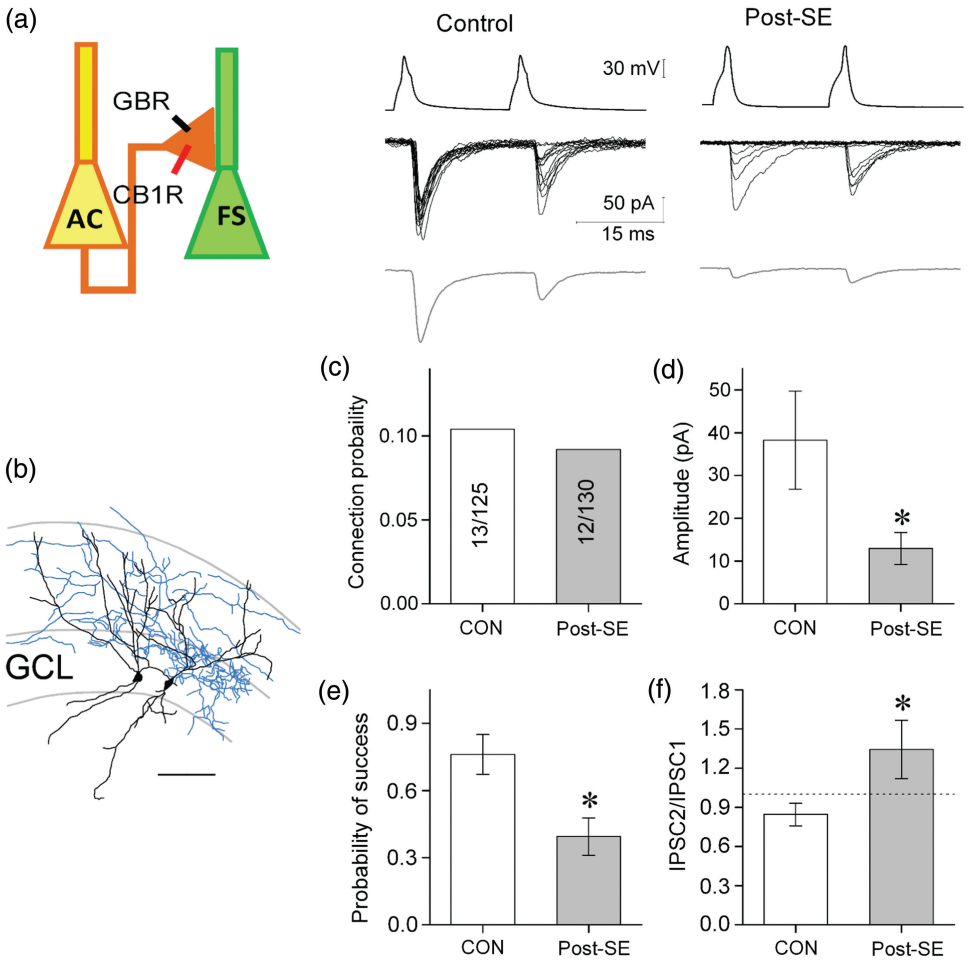


**Figure 4.** Status epilepticus reduces reliability of AC-IN synapses to FS-BC. (*a*) Schematic shows AC-IN→FS-BC recording condition (left panel). Presence of $GABA_BR$ (GBR) and cannabinoid receptor type 1 ($CB_1R$) on the AC-IN (AC) presynaptic terminal are illustrated. Representative traces from presynaptic AC-IN (above, 50 Hz), unitary IPSCs (30 individual sweeps, middle), and average uIPSC (below) in synaptically connected FS-BCs from control (middle panel) and post-SE (right panel) rats. (*b*) Neurolucida reconstruction (axon in blue, scale bar = 100 µm) of a representative AC-IN→FS-BC pair (right panel). Note the TML-like morphology of the AC-IN with sparse axons extending through the entire extent of molecule layer while FS-BC shows dense axonal arbors in the granule cell layer. GCL: granule cell layer. (*c–f*) Summary plots of the connection probability (*c*), average uIPSC amplitude including failures (*d*), probability of success (*e*), and paired pulse ratio at 50 Hz (*f*) at AC-IN→FS-BC synapses (*$P < 0.05$).

probability of synaptic connections between AC-IN→FS-BC pairs was similar in control and post-SE rats (Fig. 4*c*: control: 10.4%, 13/125 pairs, post-SE: 9.2%, 12/130 pairs, $P > 0.05$, $\chi^2$ test). However, the average amplitude of AC-IN→FS-BC uIPSCs including failures was reduced after SE (Fig. 4*d*, in pA, control: 38.3 ± 11.5, post-SE: 12.9 ± 3.7, 11 pairs each, $P < 0.05$, *U*-test). The decrease in average amplitude resulted from a significant reduction in release probability (Fig. 4*e*: control: 0.76 ± 0.09; post-SE: 0.39 ± 0.08, $n = 11$ pairs each, $P < 0.05$, *U*-test). The uIPSC amplitude potency (amplitude of successful synaptic events) was not significantly different between control and post-SE pairs (control: 50.1 ± 12.4 pA, post-SE: 32.7 ± 7.7 pA, 11 pairs each, $P > 0.05$, *U*-test, data not shown). These data demonstrate that a functional reduction in synaptic release mediates post-SE decrease in average uISPC amplitude at AC-IN→FS-BC synapses. In controls, AC-IN→FS-BC synapses showed a mild short-term depression during 50-Hz stimulation (Fig. 4*f*, $IPSP_2/IPSP_1$, control: 0.84 ± 0.09, $n = 11$ pairs). However, following SE, the short-term depression between AC-IN→FS-BC synapses was reduced and converted to paired- and multipulse facilitation (Fig. 4*f*, $IPSP_2/IPSP_1$, post-SE 1.34 ± 0.22, $n = 11$ pairs, $P < 0.05$, *t*-test; Supplementary Fig. 1*c*,*d*), consistent with the post-SE decrease in success rate. These data demonstrate that SE reduces the efficacy and alters the temporal dynamics of unitary AC-IN inputs to FS-BCs.

## Post-SE Increase in $GABA_B$ Tone at AC-IN→FS-BC Synapses

After identifying that SE reduced AC-IN→FS-BC synaptic release, we investigated the possible underlying mechanisms. Previous studies have demonstrated cell-type-specific expression of $GABA_B$ receptors ($GABA_BR$) in neurons expressing various neurochemical markers including CCK, and a selective lack of $GABA_BR$ in PV-expressing interneurons (Sloviter et al. 1999). Recent studies have identified an increase in $GABA_BR$ function in the hippocampus in an experimental model of epilepsy in mice (Dugladze et al. 2013). Since activation of presynaptic $GABA_B$ autoreceptors can reduce synaptic release, we examined whether an increase in $GABA_BR$ function contributes to the post-SE decrease in reliability of AC-IN→FS-BC synapses. A saturating concentration of the $GABA_BR$ antagonist SCH50911 (10 µM) (Wu and Saggau 1995) increased reliability of transmission at AC-IN→FS-BC synapses in both control (Fig. 5*a*,*b*, probability of success: 0.59 ± 0.14 before, 0.69 ± 0.14 after, $n = 6$ pairs, $P < 0.05$, paired *t*-test) and post-SE

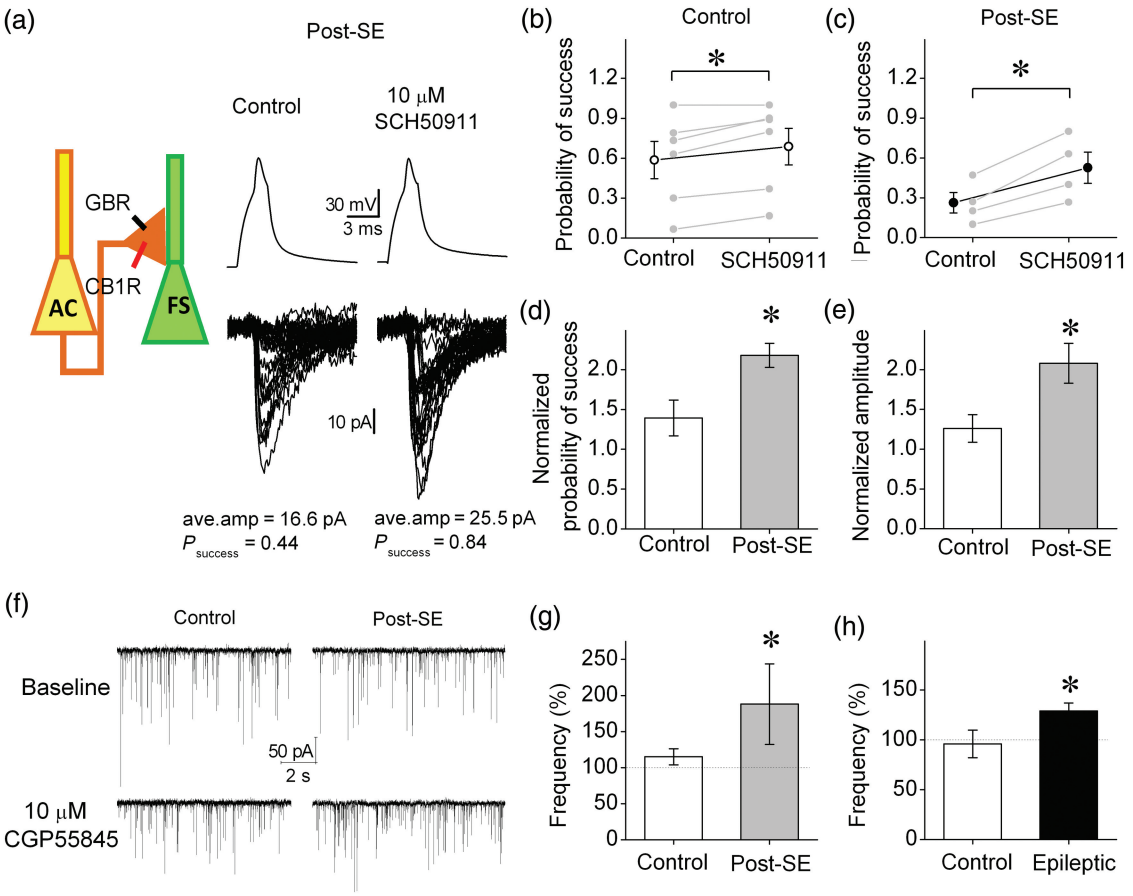


**Figure 5.** Enhanced basal presynaptic $GABA_BR$ activity reduces inhibition at AC-IN synapses to FS-BCs after SE. (*a*) Schematic of recording condition (left) illustrates $GABA_BR$ (GBR) and cannabinoid receptor type 1 ($CB_1R$) on the AC-IN presynaptic terminal. Representative traces of an AC-IN→FS-BC pair from a post-SE rat show action potentials in the presynaptic AC-IN (above) and FS-BC uIPSCs evoked by 30 consecutive sweeps (below). Responses before (middle) and after (right) perfusion of $GABA_B$ receptor antagonist 10 μM SCH50911 are illustrated. The average amplitude and probability of success ($P_{success}$) are indicated below the respective traces (*b*,*c*) Summary plots show that SCH50911 increases success rate in AC-IN→FS-BC pairs from control (*b*,) and post-SE rats (*c*). (*d*,*e*) Summary plots of success rate (*d*) and average uIPSC amplitude (*e*) in SCH50911, normalized to values before drug application in interneuronal pairs from control and post-SE rats. (*f*) Representative current traces show sIPSCs in control (middle) and post-SE (right) FS-BCs. Baseline recordings prior to drug application (above) and in 10 μM CGP55845 (below) are shown. (*g*) Summary of sIPSC frequency in CGP55845 as a percent of corresponding baseline values in control and post-SE rats (*$P < 0.05$, *t*-test). (h) Summary of sIPSC frequency in CGP55845 as a percent of corresponding baseline values in control and epileptic rats (*$P < 0.05$, *t*-test).

rats (Fig. 5*a*,*c*, probability of success: 0.26 ± 0.08 before and 0.52 ± 0.12 after, $n = 4$ pairs, $P < 0.05$, paired *t*-test). Notably, SCH50911 increased AC-IN→FS-BC synaptic success rate to a greater extent after SE than in controls (Fig. 5*d*, probability of success in SCH50911 normalized to aCSF, control: 1.39 ± 0.23, $n = 6$ pairs; post-SE: 2.18 ± 0.15, $n = 4$ pairs, $P < 0.05$, *t*-test). When $GABA_BR$ activity was suppressed, the success rate at AC-IN→FS-BC synapses was not different in slices from control and post-SE rats (probability of success in SCH50911, control: 0.69 ± 0.14, $n = 6$ pairs; post-SE: 0.52 ± 0.12, $n = 4$ pairs, $P = 0.39$, *t*-test). Moreover, uIPSC success rate in AC-IN→FS-BC pairs from post-SE rats recorded in SCH50911 was not different from the success rate in pairs from control rats recorded in the absence SCH50911 (success rate: control in vehicle: 0.59 ± 0.14, $n = 6$ pairs; post-SE in SCH50911: 0.52 ± 0.12, $n = 4$ pairs, $P = 0.74$, *t*-test). These data indicate that enhanced $GABA_BR$ function underlies the post-SE decrease in synaptic release at AC-IN→FS-BC synapses and that blocking $GABA_BR$ could restore this inhibitory deficit. As expected based on changes in release probability, SCH50911 also caused greater increase in the average uIPSC amplitude at AC-IN→FS-BC synapses after SE (Fig. 5*e*: uIPSC average amplitude in SCH50911 normalized to average amplitude in aCSF, control: 1.26 ± 0.17, $n = 6$ pairs; post-SE: 2.08 ± 0.25, $n = 4$ pairs, $P < 0.05$, *t*-test). In contrast to AC-IN→FS-BC pairs, SCH50911 failed to increase success rate and amplitude of homotypic FS-BCs synapses (Supplementary Fig. 2) indicating the absence of basal $GABA_B$ modulation of FS-BC synapses. Together, these data demonstrate cell-type-specific steady-state $GABA_BR$ modulation of FS-BC synaptic inputs from AC-INs.

In earlier studies examining pyramidal cell inhibition, blocking $GABA_BR$ was shown to reduce paired pulse depression (i.e., increase paired pulse ratio defined as the ratio of amplitude of IPSC2 to IPSC1) after SE (Dugladze et al. 2013). On this basis, it was suggested that $GABA_B$ autoreceptors contribute significantly to paired pulse depression of IPSCs in CA3 pyramidal cells. In 4 of 4 post-SE AC-IN→FS-BC pairs, we found that SCH50911 reduced paired pulse ratio (i.e., increased paired pulse depression; IPSC2/IPSC1 in SCH50911 normalized to IPSC2/IPSC1 before SCH50911 perfusion: 70.3 ± 7.4%, $P = 0.02$, paired *t*-test, data not shown). Thus, our data are consistent with $GABA_B$ blockers increasing baseline synaptic release probability of the first IPSC and contributing to greater paired pulse depression of AC-

IN→FS-BC synapses after SE and differ from the enhanced $GABA_B$ autoreceptors function observed in CA3 pyramidal cells after SE (Dugladze et al. 2013).

Since $GABA_BR$ contribute to the decrease in reliability at AC-IN→FS-BC synapses after SE, we reasoned that $GABA_BR$ antagonists would cause a greater increase in sIPSC frequency in FS-BCs from post-SE rats. In order to minimize the recording time, a fast-acting high-affinity $GABA_BR$ antagonist CGP55845 (10 μM) was used at a saturating concentration to examine $GABA_BR$ regulation of FS-BC sIPSCs. In agreement with the post-SE increase in baseline $GABA_B$ modulation of synaptic release (Fig. 5*a*–*e*), CGP55845 (10 μM) enhanced sIPSC frequency in FS-BCs from post-SE and not control rats (Fig. 5*f*,*g*, frequency normalized to aCSF: control 115 ± 11%, $n = 9$ neurons, $P > 0.05$, paired *t*-test; post-SE 188 ± 56%, $n = 10$ neurons, $P < 0.05$, paired *t*-test). Moreover, the post-SE decrease in FS-BC sIPSC frequency (Fig. 2*b*) was abolished in CGP55845 (Fig. 5*f*,*g*, frequency in CGP55845 in Hz: control: 2.94 ± 0.35, $n = 9$ neurons; post-SE: 4.56 ± 1.14, $n = 10$ neurons, $P = 0.2$, *t*-test). These data support a central role for $GABA_B$-mediated suppression of synaptic release in the functional reduction of inhibitory inputs to FS-BCs after SE. In contrast to the antagonist, the $GABA_B$ agonist baclofen (10 μM) reduced both FS-BC sIPSC frequency and amplitude in control and post-SE rats (Supplementary Fig. 3). If AC-IN→FS-BC synapses are the principal target for presynaptic $GABA_B$ modulation of release, we expected that baclofen effects would be reduced after SE. However, contrary to the expected results, baclofen reduction of FS-BC sIPSC frequency was significantly greater after SE (Supplementary Fig. 3*a*, *b*, % of baseline, control: 76.1 ± 4.6, $n = 10$ cells; post-SE: 51.2 ± 4.3, $n = 9$ cells, $P < 0.05$, *t*-test). These data suggest that, in addition to AC-IN inputs, baclofen may suppress release at synapses from other interneuronal classes that provide synaptic inputs to FS-BCs. Baclofen suppression of FS-BC sIPSC amplitude was unchanged after SE (Supplementary Fig. 3*c*, % of baseline, control: 90.6 ± 7.6, $n = 10$ cells; post-SE: 91.1 ± 9, $n = 9$ cells, $P > 0.05$, *t*-test). Thus, although steady-state $GABA_B$ modulation of release may be dominant at AC-IN→FS-BC synapses, post-SE increase in presynaptic $GABA_BR$ function is not limited to AC-IN synapses on FS-BCs.

## Reorganization of FS-BC Synaptic Inhibition in Epileptic Rats

To determine if the changes in FS-BC synaptic inhibition observed in the latent period of epileptogenesis 1 week after SE persist with disease progression, we examined FS-BCs from a cohort of epileptic rats (see Materials and Methods) and age-matched controls. The post-SE decrease in FS-BC sIPSC frequency (Fig. 2*b*,*c*) persisted in epileptic rats (in Hz, control: $\text{median}_{(IQR)} = 4.13_{(1.84–10.47)}$, $n = 22$ neurons; epileptic: $\text{median}_{(IQR)} = 3.33_{(1.41–8.53)}$, $n = 27$ neurons, $P < 0.05$, K-S test, data not shown). However, FS-BC sIPSC amplitude increased in epileptic rats (in pA, control: $\text{median}_{(IQR)} = 18.51_{(12.06–27.02)}$, $n = 22$ neurons; epileptic: $\text{median}_{(IQR)} = 21.89_{(14.42–35.18)}$, $n = 27$ neurons, $P < 0.05$, K-S test, data not shown). Interestingly, FS-BC mIPSC frequency was similar in control and epileptic rats (in Hz, control: $\text{median}_{(IQR)} = 1.37_{(0.65–3.11)}$, $n = 11$ neurons; epileptic: $\text{median}_{(IQR)} = 1.42_{(0.59–3.33)}$, $n = 11$ neurons, $P > 0.05$, K-S test, data not shown). It is possible that network structural changes including sprouting of interneuronal terminals in epilepsy (Zhang et al. 2009; Peng et al. 2013) contribute to recovery mIPSC frequency with disease progression. FS-BC mIPSC amplitude was decreased in epileptic rats (in pA, control $\text{median}_{(IQR)} = 75.42_{(56.58–100.08)}$, $n = 11$ neurons; epileptic $\text{median}_{(IQR)} = 66.46_{(50.6–91.35)}$, $n = 11$ neurons, $P < 0.05$, K-S test, data not shown). The apparent recovery of mIPSC frequency, while sIPSC frequency remained reduced in epileptic rats indicates that, even though network reorganization may restore FS-BC synaptic inputs, spontaneous synaptic inhibition of FS-BCs remains functionally compromised in epilepsy. Yet, as in post-SE rats, baclofen suppression of FS-BC sIPSC frequency was enhanced (Supplementary Fig. 3*d*, % of baseline, control: 75.2 ± 7.6, $n = 7$ cells; epileptic: 54.1 ± 4.6, $n = 11$ cells, $P < 0.05$, *t*-test) while modulation of amplitude remained unaltered in epileptic rats (Supplementary Fig. 3*e*, % of baseline, control: 85.8 ± 5, $n = 7$ cells; epileptic: 82.4 ± 5.5, $n = 11$ cells, $P > 0.05$, *t*-test) indicating persistent post-SE increase in $GABA_BR$ at interneuronal terminals. More importantly, similar to results obtained in FS-BCs from post-SE rats (Fig. 5*g*), CGP55845 (10 μM) continued to selectively increase sIPSC frequency in FS-BCs from epileptic rats (Fig. 5*h*, frequency normalized to aCSF, control: 95.9 ± 13.9%, $n = 9$ neurons, $P > 0.05$, paired *t*-test; epileptic: 129 ± 8%, $n = 9$ neurons, $P < 0.05$, paired *t*-test). Furthermore, CGP55845 eliminated the decrease in FS-BC sIPSC frequency in epileptic rats (frequency in CGP55845 in Hz: control: 4.1 ± 1.2, $n = 9$ neurons; post-SE: 5.1 ± 0.8, $n = 9$ neurons, $P = 0.49$, *t*-test, data not shown). These data show that enhanced baseline $GABA_BR$-mediated suppression of synaptic release contributes substantively to the decrease in sIPSC frequency in FS-BCs from epileptic rats.

## Reduced $CB_1R$-Sensitive Inhibition of FS-BCs in Epilepsy

TML cells and CCK-positive HICAP cells express $CB_1R$ on their axon terminals (Morozov et al. 2009; Yu et al. 2015). Activation of $CB_1R$ is known to suppress synaptic release in several brain regions (Acsady et al. 2000; Karson et al. 2009). Since $GABA_BR$ expression is not limited to AC-INs (Sloviter et al. 1999; Booker et al. 2013), we sought to utilize the selective sensitivity of AC-IN synapses to $CB_1R$, to examine if the proportion FS-BC sIPSCs arising from AC-IN inputs is different in control and post-SE rats. However, whether $CB_1R$ modulates baseline AC-IN transmission to dentate FS-BCs remains untested. In AC-IN→FS-BC pairs, the $CB_1R$ antagonist AM251 (10 μM) consistently increased both uIPSC success rate and average amplitude in 5 of 5 cell pairs tested (Supplementary Fig. 4*a*–*c*, including the morphologically identified TML→FS-BC pair illustrated in Fig. 4*a*). The increase in synaptic release by AM251 demonstrates baseline endocannabinoid suppression at AC-IN→FS-BC synapses. In contrast, homotypic FS-BC synapses were not modulated by AM251 (Supplementary Fig. 4*d*–*f*).

Having confirmed that $CB_1R$ antagonist selectively modulates release at AC-IN and not FS-BC synapses on FS-BCs, we used the $CB_1R$ agonist, WIN55212–2 (5 μM) which has been adopted by earlier studies to block $CB_1R$-sensitive synaptic events (Wyeth et al. 2010; Sun et al. 2014), to determine the contribution of $CB_1R$-sensitive AC-IN inputs to FS-BC synaptic inhibition. Use of the $CB_1R$ agonist WIN55212-2 (5 μM) to suppress $CB_1R$-sensitive events, rather than an antagonist, eliminates potential confounds that may arise from differences in baseline $CB_1R$ expression or activity between experimental groups. Since AC-IN→FS-BC synapses are modulated by $CB_1R$, post-SE decrease in AC-IN inputs to FS-BCs would be expected to reduce the proportion FS-BC sIPSCs blocked by the $CB_1R$ agonist. WIN55212-2 reduced FS-BC sIPSC frequency in both control and post-SE rats (Fig. 6*a*–*d*, frequency in Hz, control: $\text{median}_{(IQR)} = 4.25_{(1.51–10.24)}$ before vs. $2.71_{(1.11–7.2)}$ after WIN55212-2, $n = 7$, $P < 0.05$; post-SE: $\text{median}_{(IQR)} = 4.19_{(1.94–8.83)}$ before and $3.01_{(1.31–6.89)}$ after WIN55212-2, $n = 8$, $P < 0.05$, K-S test). Importantly, as predicted, WIN55212-2 suppression of FS-BC sIPSC frequency was significantly reduced after SE (Fig. 6*e*, % of baseline, control: 62.9 ± 4.4%, $n = 7$; post-SE: 78.2 ±

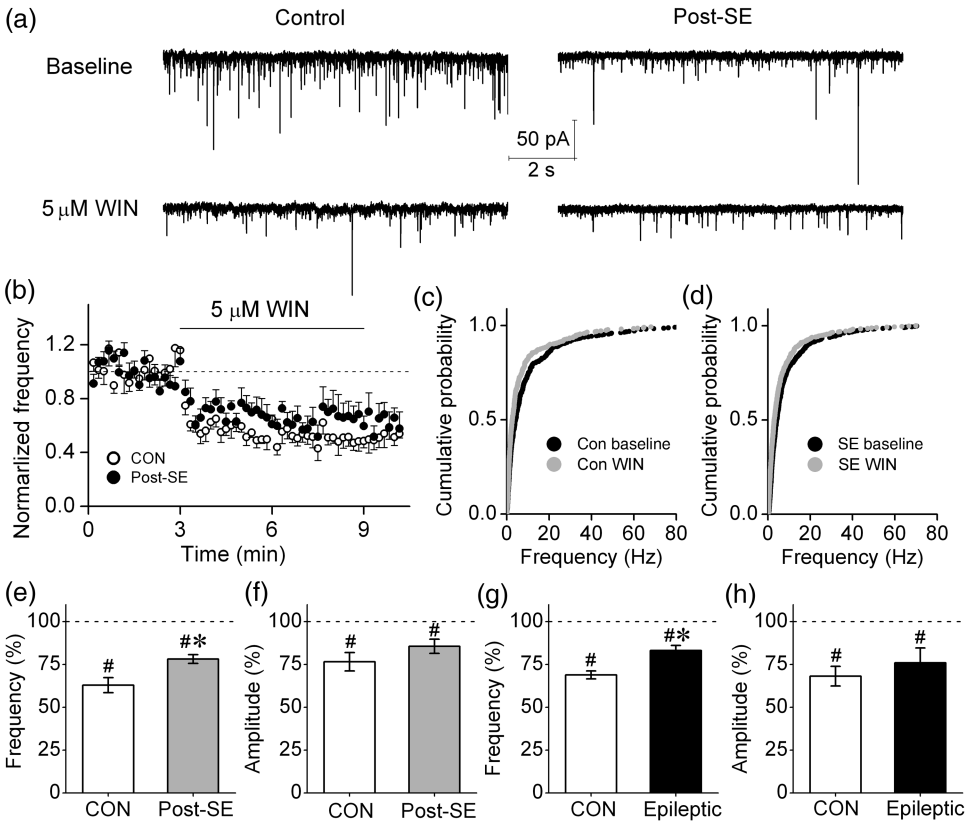


**Figure 6.** $CB_1R$-sensitive FS-BC sIPSCs are decreased in post-SE and epileptic rats. (*a*) Representative traces illustrate FS-BC sIPSCs from control (left) and post-SE (right) rats. Segments show recordings under baseline conditions (above) and in 5 μM WIN55212-2 (below). (*b*) Time course of mean sIPSC frequency of 10 s segments of data (normalized to baseline) during application of WIN55212-2 in FS-BCs from control and post-SE rats. (*c*,*d*) Cumulative probability plots compare FS-BC sIPSC instantaneous frequency during baseline recordings and in WIN55212-2 in control (*c*) and post-SE rats (*d*). (*e*,*f*) Plot of sIPSC frequency (*e*) and amplitude (*f*) in WIN55212-2, normalized to corresponding baseline values, in FS-BCs from control and post-SE rats. (*g*,*h*) Summary histogram of FS-BC sIPSC frequency (*g*) and amplitude (*h*) in WIN55212-2, normalized to corresponding baseline values, in slices from control and epileptic rats ($^{\#}P < 0.05$ compared with baseline by paired *t*-test; $^{*}P < 0.05$, compared with age-matched control by *t*-test).

2.5%, $n = 8$, $P < 0.05$, *t*-test). WIN55212-2 reduced FS-BC sIPSC amplitude to a similar extent in both control and post-SE rats (Fig. 6*f*, % of baseline, control 76.6 ± 5.4%, $n = 7$; post-SE: 85.6 ± 4.1%, $n = 8$, $P > 0.05$, *t*-test). Comparison of the effects of the $GABA_BR$ agonist (baclofen) and $CB_1R$ agonist (WIN 55212-2) on FS-BC sIPSC frequency showed that baclofen suppressed a greater proportion of FS-BC sIPSCs than WIN 55212-2 in post-SE rats (frequency as % of respective baseline, baclofen: 51.2 ± 4.3%, $n = 9$, WIN55212-2: 78.2 ± 2.5%, $n = 8$, $P < 0.05$). These data confirm that baclofen effects are not limited to $CB_1R$-sensitive AC-IN→FS-BC synapses.

As observed 1 week after SE, WIN55212-2 (5 μM) continued to suppress fewer FS-BC sIPSC in epileptic rats (Fig. 6*g*, % of baseline, control: 69 ± 2.3%, $n = 4$; epileptic: 83.2 ± 3%, $n = 5$, $P < 0.05$, *t*-test). WIN 55212-2 suppression of FS-BC sIPSC amplitude remained similar in control and epileptic rats (Fig. 6*h*, % of baseline, control: 68.2 ± 5.7%, $n = 4$; epileptic: 76 ± 8.6%, $n = 5$, $P = 0.48$, *t*-test). Moreover, baclofen still suppressed a greater proportion of FS-BC sIPSCs in epileptic rats than WIN55212-2 (frequency as % of respective baseline, baclofen: 54.1 ± 4.6%, $n = 11$, WIN 55212-2: 83.2 ± 3%, $n = 5$, $P < 0.05$, *t*-test). Thus, $CB_1R$-sensitive heterotypic AC-IN→FS-BC inhibition is compromised within a week after SE and remains reduced in epileptic rats.

Immunostaining showed that the number of CCK-expressing neurons in the hilar-granule cell layer border was not decreased in sections from post-SE rats (Supplementary Fig. 5*a*,*b*, number of cells in ROI per section, control: 33.3 ± 2.5; post-SE: 29 ± 3.8, $n = 18$ sections from 3 rats each, $P > 0.05$, *t*-test) and epileptic rats (Supplementary Fig. 5*c*,*d*, number of cells in ROI per section, control: 27.0 ± 2.6; epileptic: 27 ± 2.88.5, $n = 15$ sections from 3 rats each, $P > 0.05$, *t*-test). These findings are consistent with earlier reposts following electrically induced SE and subsequent epilepsy (Sun et al. 2007). Moreover, $CB_1R$-expressing interneurons and terminals are not reduced in epileptic rats (Magloczky et al. 2010). Taken together, our histological and physiological data indicate that a $GABA_BR$-mediated functional, rather than a structural, decrease in AC-IN synaptic inputs to FS-BCs underlies the persistent decrease in $CB_1R$-sensitive synaptic inhibition of FS-BC in epileptic rats.

## Reduced Reliability of AC-IN→FS-BC Synapses Alters Network Oscillations

Deficits in memory processing constitute a significant co-morbidity in epilepsy (Chauviere et al. 2009; Kitchigina et al. 2013). Inhibitory neuronal networks underlie brain rhythms which are crucial for memory formation (Wang 2010). In network simulations, inhibition from adapting interneurons is critical for maintaining theta oscillations in the presence of network gamma rhythms (White et al. 2000; Whittington et al. 2000; Bartos et al. 2002; Rotstein et al. 2005; Vida et al. 2006). Thus, the post-SE changes in interneuronal inputs observed in this study could undermine theta-gamma oscillations leading to memory

deficits. In the dentate gyrus, the basic circuit for generating theta-gamma oscillations involves theta-modulated entorhinal glutamatergic drive and the local dentate inhibitory networks (Pernia-Andrade and Jonas 2014). We adopted network simulations to examine if the experimentally identified post-SE reduction in AC-IN→FS-BC reliability can impact theta-gamma oscillations. Use of simulations allows for highly controlled analysis and eliminates confounds arising from the multitude biological changes occurring during epileptogenesis. Our FS-BCs network model (Proddutur et al. 2013) was expanded by including biophysically based AC-IN models (Supplementary Fig. 6 and Table 1).

Heterogeneous interneuron-only networks had FS-BC→FS-BC, AC-IN→AC-IN, and AC-IN→FS-BC synapses (Schematic in Fig. 7*a*). Network activity was initiated by introducing theta-modulated current injection ($I_{inj\text{-}\theta}$) with start times staggered to generate variability in cell firing (see Materials and Methods). In the absence of AC-IN activation, FS-BC networks activated by $I_{inj\text{-}\theta}$ developed coherent firing at 40–80 Hz (Fig. 7*a*,*b*), similar to networks activated by constant current or synaptic inputs (Bartos et al. 2002; Proddutur et al. 2013). Introducing $I_{inj\text{-}\theta}$ to AC-INs staggered between 300 and 337.5 ms, resulted in establishment of heterotypic networks with variability in firing. In "control" networks, with AC-IN→FS-BC synaptic release probability ($P_{release(AC\text{-}IN\rightarrow FS\text{-}BC)}$) set to 0.8 (schematic in Fig. 7*a*), FS-BCs continued to show coherent gamma frequency firing following activation of AC-INs (Fig. 7*a*,*c*). FS-BC-derived LFPs showed a distinct theta frequency-power peak (Fig. 7*f*, inset), likely because model AC-INs with membrane sag and low firing frequency phase lock better with theta frequency inputs as proposed previously (White et al. 2000; Rotstein et al. 2005). The biologically based slower kinetics of AC-IN→FS-BC synapses may also have contributed to theta frequency coherence in network firing. In "post-SE" networks with $P_{release(AC\text{-}IN\rightarrow FS\text{-}BC)}$ set to 0.3 (schematic in Fig. 7*b*), FS-BCs fired with greater coherence (Fig. 7*b*,*d*,*e*; effect of $P_{release(AC\text{-}IN\rightarrow FS\text{-}BC)}$ on coherence $F_{1,8} = F_{1,8} = 4543.64$, $P < 0.05$ by TW-RM-ANOVA). Power spectra of FS-BC-derived LFPs showed peaks at both theta and gamma frequencies (Fig. 7*f*). However, the power of the theta peak in FS-BC-derived LFPs was reduced and gamma power increased in post-SE networks (Fig. 7*g*,*h*; effect of $P_{release(AC\text{-}IN\rightarrow FS\text{-}BC)}$ on theta power $F_{1,8} = 55.04$, $P < 0.05$, gamma power $F_{1,8} = 99.26$, $P < 0.05$ by TW-RM-ANOVA). Output measures from post-SE networks were normalized to structurally identical control networks for analysis. Decreasing $P_{release(AC\text{-}IN\rightarrow FS\text{-}BC)}$ consistently enhanced coherence of FS-BC firing and gamma power and reduced theta power in FS-BC-derived LFPs over a range of $I_{inj\text{-}\theta}$ tested (Fig. 7*e*–*h*) as a consequence of the reduction in AC-IN influence on FS-BC activity moving the network activity closer to what is observed in isolated FS-BC networks. Additionally, as illustrated by phase-amplitude histograms (Fig. 7*i*,*j*), the difference between gamma amplitude maximum and minimum over a theta cycle was reduced in post-SE networks indicating decreased coupling between gamma amplitude and theta phase in "post-SE" networks. Moreover, theta-gamma coupling quantified using an entropy-based MI (Tort et al. 2007, 2010) was significantly reduced in networks with the post-SE reduction in $P_{release(AC\text{-}IN\rightarrow FS\text{-}BC)}$ (Fig. 7*k*: effect of $P_{release}$ on MI, $F_{1,8} = 70.92$, $P < 0.05$ by TW-RM-ANOVA). Additional control simulations were performed to verify the robustness of the findings. In simulations including FS-BC→AC-IN synapses with the same conductance and kinetics as FS-BC→FS-BC synapses (Savanthrapadian et al. 2014), reducing $P_{release(AC\text{-}IN\rightarrow FS\text{-}BC)}$ still enhanced gamma power and reduced theta power of FS-BC-derived LFPs (not shown). Similarly, the ability of reduced $P_{release(AC\text{-}IN\rightarrow FS\text{-}BC)}$ to enhance gamma power and reduce theta power persisted even when FS-BCs received constant current injections devoid of theta frequency modulation (not shown).

In addition to the interneuron-only networks above, we implemented E-I networks that include biologically based granule cell models (Fig. 8, Santhakumar et al. 2005). All model cells received $I_{inj\text{-}\theta}$ with variable start times (see Materials and Methods). As with interneuron-only heterogeneous networks, reducing $P_{release(AC\text{-}IN\rightarrow FS\text{-}BC)}$ reduced theta-gamma coupling in FS-BCs in the E-I networks (Fig. 8*c*–*e*, effect of $P_{release(AC\text{-}IN\rightarrow FS\text{-}BC)}$ on MI, $F_{1,8} = 169.04$, $P < 0.05$ by TW-RM-ANOVA). Decreasing $P_{release(AC\text{-}IN\rightarrow FS\text{-}BC)}$ caused a robust enhancement in gamma power and reduced power of theta frequency oscillations in granule cell-derived LFPs from E-I networks (Fig. 8*f*–*i*; effect of $P_{release(AC\text{-}IN\rightarrow FS\text{-}BC)}$ on theta power: $F_{1,8} = 35.00$, $P < 0.05$, gamma power: $F_{1,8} = 22.72$, $P < 0.05$ by TW-RM-ANOVA). Together, the network simulations revealed that the experimentally identified reduction in AC-IN→FS-BC reliability consistently enhanced gamma power, reduced theta power, and compromised dentate theta-gamma coupling.

## Discussion

Studies examining interneuronal connectional features have demonstrated the role of cell-type-specific interneuronal connectivity in shaping network activity patterns. However, few studies have examined changes in mutual connections among interneurons in neurological disease (Ma and Prince 2012; Zhou and Roper 2014). Using technically challenging, paired interneuronal recordings, we demonstrate that the perisomatic inhibitory network in the dentate gyrus, a circuit that gates the spread of seizure activity (Coulter and Carlson 2007), is fundamentally altered following SE, by preserving homotypic synaptic connections and reducing heterotypic inhibition to dentate FS-BCs. Mechanistically, we identify that an increase in basal $GABA_B$ tone, specifically at $CB_1R$-sensitive synapses on FS-BCs, contributes to the functional decrease in heterotypic inhibition of FS-BCs after SE. Using pharmacological approaches as an alternative to paired recordings, which decrease in feasibility with age and disease progression, we demonstrate an early and persistent $GABA_B$-dependent functional suppression of FS-BC inhibition and reduction in $CB_1R$-sensitive inputs to FS-BCs persists in post-SE and spontaneously epileptic rats. Our biophysically based network simulations reveal that the experimentally determined selective increase in transmission failures at AC-IN→FS-BC synapses augments gamma power and compromises theta power and cross-frequency coupling. These changes could contribute to the disruption of memory formation and recall (Fell et al. 2001; Chauviere et al. 2009).

Our data indicate that the characteristic strength and reliability of homotypic FS-BC synapses remains unchanged following SE. These findings differ from the decrease in reliability of FS-BC inputs to GCs in epilepsy (Zhang and Buckmaster 2009) indicating independent regulation of FS-BC synaptic release to FS-BCs and GCs. The selective reduction in heterotypic inputs to FS-BCs would lead to functional isolation of FS-BC networks and potentially modify network activity patterns during epileptogenesis. Additionally, the resulting decrease in FS-BC proximal dendritic input heterogeneity after SE could alter FS-BC excitability (Aradi et al. 2004). As in the cortex and hippocampus (Freund 2003; Armstrong and Soltesz 2012), we find cell-specific differences with AC-IN, and not FS-BC, synapses under basal $GABA_B$ and $CB_1R$ regulation of release. Since $CB_1R$-expressing neurons receive diverse neuromodulatory inputs (Armstrong and Soltesz

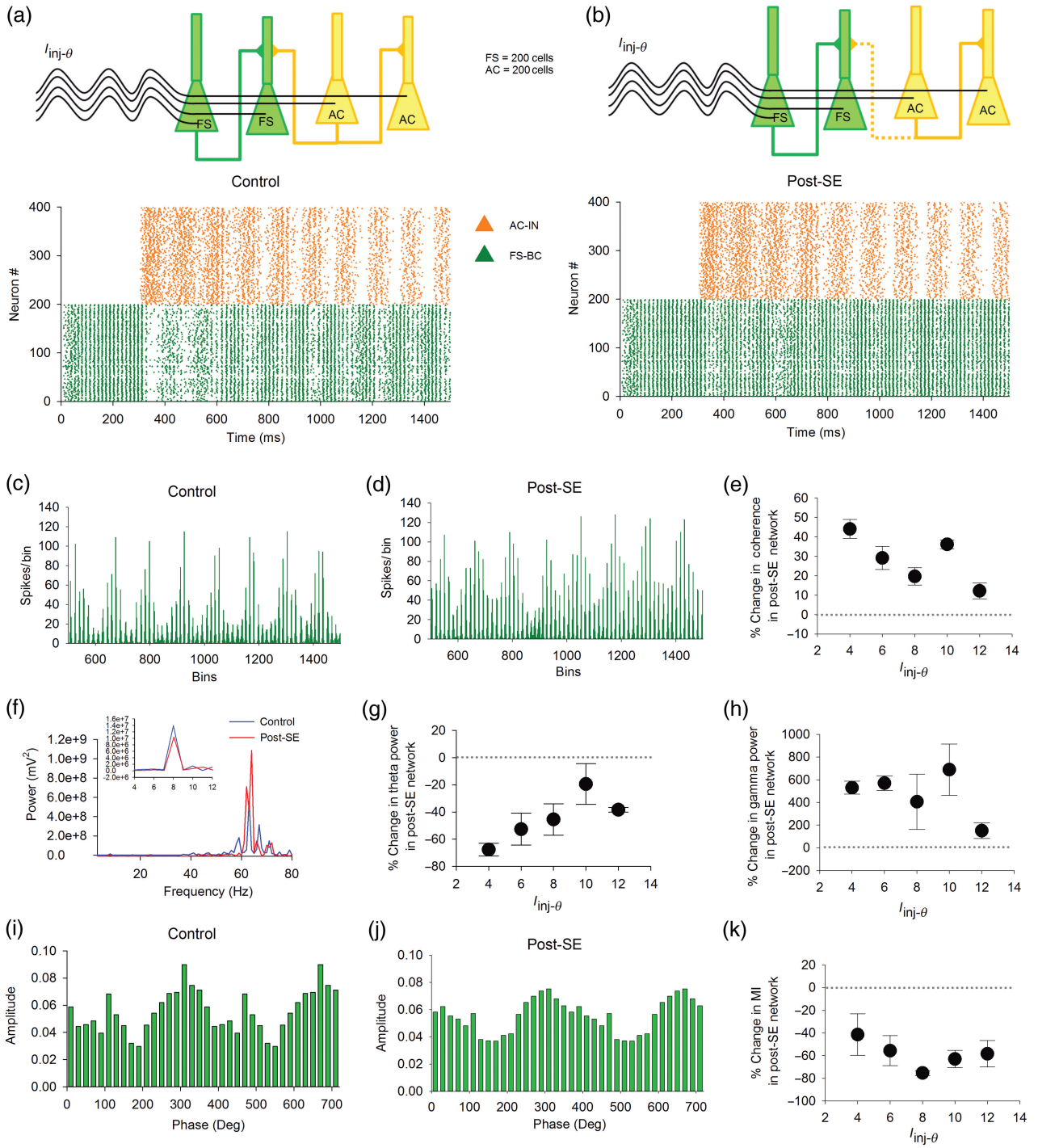


**Figure 7.** Decrease in heterotypic FS-BC inhibition impacts oscillation in interneuron-only network simulations. (*a*,*b*) Schematics (upper panels) show connectivity between FS-BCs (FS) and AC-INs (AC) in control (*a*) and post-SE (*b*) interneuron-only networks. Networks were activated by somatic $I_{inj-\theta}$. Dashed-line in *b* indicates post-SE decrease in AC-IN→FS-BC release probability. Representative spike raster plots (lower panels) show in FS-BCs (green) and AC-INs (orange) firing in control (*a*) and post-SE networks (*b*) during 8 Hz $I_{inj-\theta}$. (*c*,*d*) Spike frequency histogram from control (*c*) and Post-SE (*d*) networks from above. (*e*) Summary plot shows coherence in post-SE networks as a percent of coherence in corresponding structurally identical control networks activated by various values of $I_{inj-\theta}$. (*f*) Overlay of example frequency-power spectra from the control (blue) and post-SE networks (red) in *a*,*b*. Inset: frequency-power spectra in the theta frequency range. (*g*,*h*) Summary plots of theta (*g*) and gamma (*h*) peak power in post-SE networks normalized to structurally identical controls at various values of $I_{inj-\theta}$. (i,*j*) Phase-amplitude histograms illustrate modulation of gamma frequency amplitude by theta phase in control (i) and post-SE networks (*j*). (*k*) Summary scatter plot of the cross-frequency modulation index (MI) in post-SE networks presented as a percent of control.

2012), reduction in $CB_1R$-sensitive inputs to FS-BCs can isolate FS-BC-based network oscillations from activity or behavioral state-dependent modulation.

Reduction in the frequency of FS-BC spontaneous IPSCs occurs early after SE and persists in epileptic rats. Loss of dentate interneurons including somatostain-expressing presumed HIPP

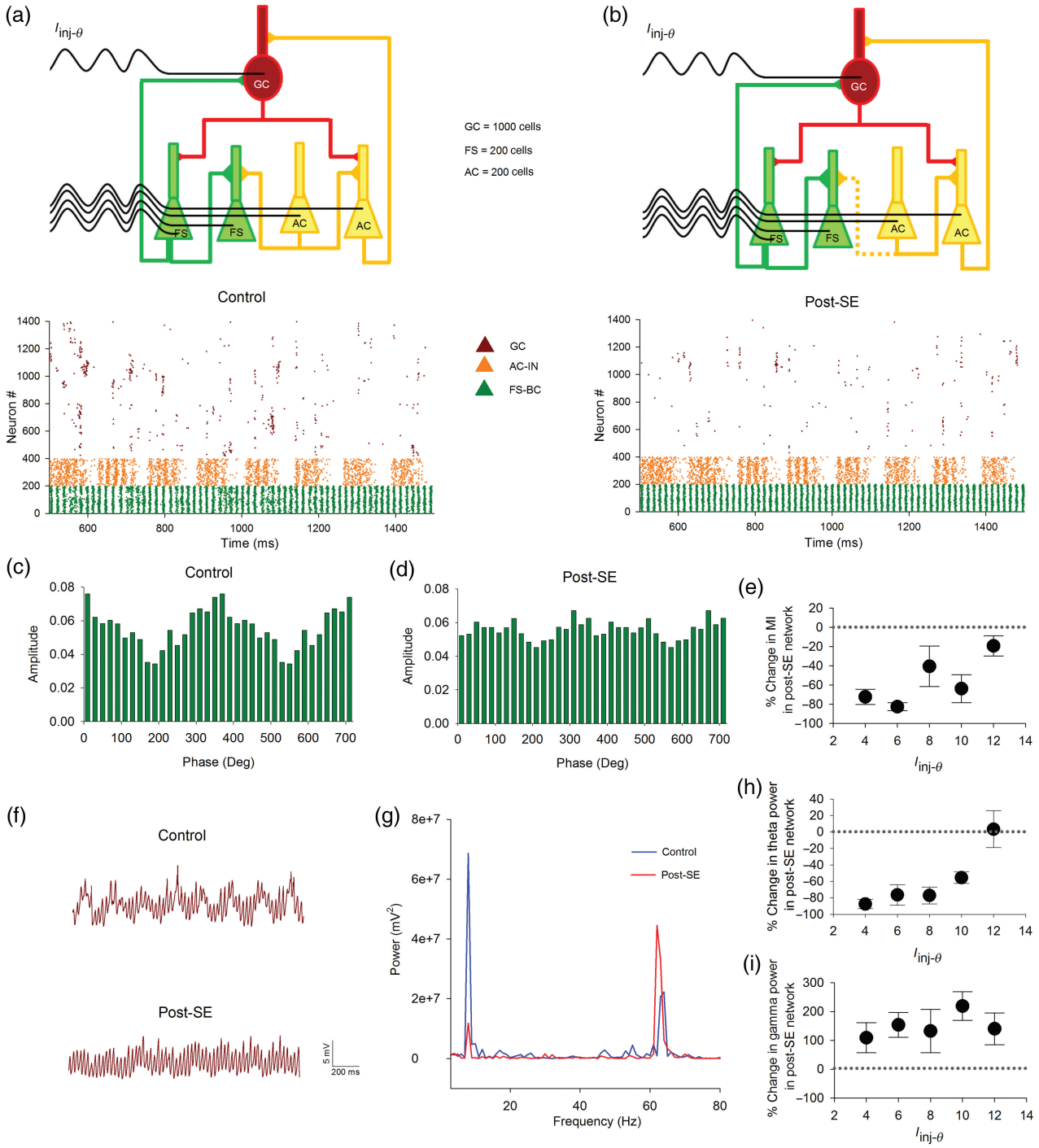


**Figure 8.** Effect of decrease in AC-IN reliability on activity patterns in E-I networks. (*a*,*b*) Schematics (upper panels) show connectivity between granule cells (GC), FS-BCs (FS) and AC-INs (AC) in control (*a*) and post-SE (*b*) E-I networks. Networks were activated by somatic $I_{inj-\theta}$ Dashed-line in b indicates post-SE decrease in AC-IN→FS-BC release probability. Representative spike raster plots (lower panels) show in FS-BCs (green) and AC-INs (orange) firing in control (*a*) and post-SE networks (*b*) during 8 Hz $I_{inj-\theta}$. (*c*,*d*) Phase-amplitude histograms of FS-BC activity illustrate change in coupling between gamma amplitude and theta phase in a control (*c*) and post-SE network (*d*). (*e*) Summary scatter plot of the cross-frequency modulation index (MI) in post-SE networks presented as a percent of control. (*f*) Illustration of granule cell-derived local field potentials (LFP) in a control (upper panel) and post-SE (lower panel) networks. (*g*) Overlay of example frequency-power spectra from control (blue) and post-SE network (red). (*h*,*i*) Summary plots of theta (*h*) and gamma (*i*) peak power in post-SE networks normalized to structurally identical controls at various values of $I_{inj-\theta}$.

cells (Obenaus et al. 1993; Kobayashi and Buckmaster 2003; Zhang et al. 2009) likely contribute to decrease in FS-BC mIPSC and sIPSC frequency after SE. However, we show that enhanced transmission failure from AC-INs to FS-BCs adds to functional disinhibition of FS-BCs. It is possible that cell-specific post-SE changes in the activity levels of interneurons contributing to large and small amplitude IPSCs result in reduced FS-BC sIPSC amplitude despite the lack of change in mIPSC amplitude.

Among the potential mechanisms for enhanced AC-IN→FS-BC synaptic failures, the ability of $GABA_B$ antagonist to reverse post-SE reduction in release (Fig. 5*a–c*) suggests that increased presynaptic $GABA_B$ tone plays a major role in regulating reliability of AC-IN→FS-BC synapses. Moreover, $GABA_B$ antagonist enhances FS-BC sIPSC frequency to control levels in both post-SE and epileptic rats providing a pharmacological target for restoring heterotypic modulation of FS-BC inhibition. The post-SE increase in basal activation of $GABA_B$ at AC-IN→FS-BC synapses reduces release probability and likely contributes to the switch in short-term plasticity from depression to facilitation (Supplementary Fig. 1). The ability of $GABA_B$ agonists to suppress a greater proportion of FS-BC sIPSCs than the $CB_1R$ agonist in post-SE rats demonstrates that SE increases $GABA_B$ receptors at $CB_1R$-insensitive synapses as well. Indeed, $GABA_BR$ are expressed in several classes of dentate interneurons including those expressing somatostatin, calretinin, and NPY (Sloviter et al. 1999) and could undergo cell-type-specific changes in expression levels in these interneuronal populations following SE. Our demonstration of post-SE increase in $GABA_B$-mediated suppression of FS-BC synaptic inhibition is consistent with recent findings in CA3 pyramidal cells in a mouse model of epilepsy (Dugladze et al. 2013).

Earlier studies in dentate GCs have demonstrated early post-SE reduction in afferent-evoked synaptic inhibition that either recovers or is enhanced at later time points (Bausch and Chavkin 1997; Buckmaster and Dudek 1997). Anatomical studies have demonstrated an early post-SE reduction in granule cell GABAergic synapses followed by an excess of GABAergic terminals in epileptic animals (Thind et al. 2010). However, granule cell sIPSC and mIPSC frequency remain reduced in epilepsy (Kobayashi and Buckmaster 2003; Shao and Dudek 2005; Sun et al. 2007). In contrast, we find that, while the post-SE reduction in FS-BC sIPSC frequency persists in epilepsy, FS-BC mIPSC frequency recovers to control levels in epileptic rats. It is possible that sprouting of inhibitory terminals mediating distal dendritic inputs in the outer molecular layer (Zhang et al. 2009; Thind et al. 2010; Peng et al. 2013) contributes to the recovery of FS-BC mIPSC frequency while decreasing mIPSC amplitude at later time points after SE. In contrast, sIPSC amplitude, which was reduced after SE, increases in epileptic rats as has been reported in GCs (Sun et al. 2014) suggesting that FS-BCs may show strengthening of proximal inputs with progression of disease. Yet, $CB_1R$ agonist consistently suppressed a smaller proportion of FS-BC sIPSCs in post-SE and epileptic rats indicating the AC-IN inhibition of FS-BCs remains reduced in epilepsy. The decrease in $CB_1R$-sensitive synaptic inhibition of FS-BCs from epileptic rats parallels findings in GCs (Sun et al. 2014). However, the persistent increase in basal $GABA_B$ tone in epileptic rats and lack of difference in FS-BC sIPSC frequency in $GABA_BR$ antagonist indicate that the functional reduction in synaptic release has a dominant role in reducing $CB_1R$-sensitive inhibition of FS-BCs in epileptic rats.

Homogeneous networks of fast-spiking dentate and hippocampal neurons generate gamma frequency oscillations, the characteristics of which are modified by changes in FS-BC synaptic and extrasynaptic inhibition (Vida et al. 2006; Proddutur et al. 2013; Yu et al. 2013). Mixed theta-gamma oscillations derive from interactions between heterogeneous inhibitory and excitatory neuronal populations and neuromodulatory inputs (Wang 2010). We find that SE undermines FS-BC inputs from adapting interneurons, which contribute to theta modulation of gamma oscillations in network simulations (White et al. 2000; Rotstein et al. 2005). While earlier studies manipulated steady-state current to model reduction in inhibitory drive (Dugladze et al. 2013), we implemented mechanistically based simulations in which release probability was manipulated to model the reduction in frequency of AC-IN inputs to FS-BCs. Reducing reliability of heterotypic inputs to FS-BCs consistently reduced network theta oscillations and could contribute to reduction in entorhinal-dentate theta coupling observed in experimental epilepsy (Froriep et al. 2012). Recent findings demonstrating that the power of pharmacologically induced CA3 gamma oscillations are increased in epilepsy and that $GABA_B$ antagonist reduces gamma power in epileptic networks (Dugladze et al. 2013) are consistent with our experimental and simulations results. Exclusion of seizure-induced excitatory sprouting, alteration in reversal potential in the "post-SE" network model and activity-dependent modulation of $CB_1R$-sensitive IPSCs limit the ability of the model to predict changes in excitability. Additionally, while individual AC-INs in our simulations did not fire on each gamma cycle or show high-frequency firing, the dynamic changes in inhibition due to post-SE changes in short-term facilitation/depression, not included in the current model, may also influence activity in biological networks. Although omission of previously reported post-SE changes in FS-BCs in our simulations may be considered a limitation, they provide the unique advantage of permitting examination of the effects of altered synaptic inhibition of FS-BCs on network oscillations without the confounding effects of known and unknown changes that cannot be eliminated in a biological system. Given the importance of theta-gamma oscillations to memory formation (Wang 2010), post-SE changes in network oscillations observed in our biologically based simulations may contribute to behavioral co-morbidities including memory deficits in seizure disorders. Since FS-BCs networks are involved in neurological disorders including schizophrenia and major depression, changes in the balance between homotypic and heterotypic inhibition of FS-BCs may play a role in behavioral symptoms associated with other neurological disorders.

## Supplementary Material

Supplementary material can be found at: http://www.cercor.oxfordjournals.org/.

## Authors' Contributions

J.Y., A.P., and B.S. performed experiments; J.Y., A.P., and B.S. analyzed data; J.Y., A.P., and V.S. interpreted results of experiments; J.Y., A.P., and F.S.E. prepared figures; J.Y., A.P., and V.S. conception and design of research; J.Y., A.P., and V.S. drafted manuscript.

## Funding

This work is supported by Epilepsy Foundation grants to J.Y. and NIH/NINDS NS069861 to V.S.

## Notes

*Conflict of Interest:* None declared.

## References

Acsady L, Katona I, Martinez-Guijarro FJ, Buzsaki G, Freund TF. 2000. Unusual target selectivity of perisomatic inhibitory cells in the hilar region of the rat hippocampus. J Neurosci. 20:6907–6919.

Aradi I, Santhakumar V, Soltesz I. 2004. Impact of heterogeneous perisomatic IPSC populations on pyramidal cell firing rates. J Neurophysiol. 91:2849–2858.

Armstrong C, Soltesz I. 2012. Basket cell dichotomy in microcircuit function. J Physiol. 590:683–694.

Bartos M, Vida I, Frotscher M, Geiger JR, Jonas P. 2001. Rapid signaling at inhibitory synapses in a dentate gyrus interneuron network. J Neurosci. 21:2687–2698.

Bartos M, Vida I, Frotscher M, Meyer A, Monyer H, Geiger JR, Jonas P. 2002. Fast synaptic inhibition promotes synchronized gamma oscillations in hippocampal interneuron networks. Proc Natl Acad Sci USA. 99:13222–13227.

Bausch SB, Chavkin C. 1997. Changes in hippocampal circuitry after pilocarpine-induced seizures as revealed by opioid receptor distribution and activation. J Neurosci. 17:477–492.

Booker SA, Gross A, Althof D, Shigemoto R, Bettler B, Frotscher M, Hearing M, Wickman K, Watanabe M, Kulik A, et al. 2013. Differential GABAB-receptor-mediated effects in perisomatic- and dendrite-targeting parvalbumin interneurons. J Neurosci. 33:7961–7974.

Bragin A, Azizyan A, Almajano J, Wilson CL, Engel J Jr. 2005. Analysis of chronic seizure onsets after intrahippocampal kainic acid injection in freely moving rats. Epilepsia. 46:1592–1598.

Bragin A, Jando G, Nadasdy Z, Hetke J, Wise K, Buzsaki G. 1995. Gamma (40–100 Hz) oscillation in the hippocampus of the behaving rat. J Neurosci. 15:47–60.

Buckmaster PS, Dudek FE. 1997. Neuron loss, granule cell axon reorganization, and functional changes in the dentate gyrus of epileptic kainate-treated rats. J Comp Neurol. 385:385–404.

Buzsáki G. 2006. Rhythms of the brain. Oxford (NY): Oxford University Press.

Chamberland S, Topolnik L. 2012. Inhibitory control of hippocampal inhibitory neurons. Front Neurosci. 6:165.

Chauviere L, Rafrafi N, Thinus-Blanc C, Bartolomei F, Esclapez M, Bernard C. 2009. Early deficits in spatial memory and theta rhythm in experimental temporal lobe epilepsy. J Neurosci. 29:5402–5410.

Coulter DA, Carlson GC. 2007. Functional regulation of the dentate gyrus by GABA-mediated inhibition. Prog Brain Res. 163:235–243.

Dugladze T, Maziashvili N, Borgers C, Gurgenidze S, Haussler U, Winkelmann A, Haas CA, Meier JC, Vida I, Kopell NJ, et al. 2013. GABA(B) autoreceptor-mediated cell type-specific reduction of inhibition in epileptic mice. Proc Natl Acad Sci USA. 110:15073–15078.

Dyhrfjeld-Johnsen J, Santhakumar V, Morgan RJ, Huerta R, Tsimring L, Soltesz I. 2007. Topological determinants of epileptogenesis in large-scale structural and functional models of the dentate gyrus derived from experimental data. J Neurophysiol. 97:1566–1587.

Fell J, Klaver P, Lehnertz K, Grunwald T, Schaller C, Elger CE, Fernandez G. 2001. Human memory formation is accompanied by rhinal-hippocampal coupling and decoupling. Nat Neurosci. 4:1259–1264.

Freund TF. 2003. Interneuron Diversity series: rhythm and mood in perisomatic inhibition. Trends Neurosci. 26:489–495.

Froriep UP, Kumar A, Cosandier-Rimele D, Haussler U, Kilias A, Haas CA, Egert U. 2012. Altered theta coupling between medial entorhinal cortex and dentate gyrus in temporal lobe epilepsy. Epilepsia. 53:1937–1947.

Han ZS, Buhl EH, Lorinczi Z, Somogyi P. 1993. A high-degree of spatial selectivity in the axonal and dendritic domains of physiologically identified local-circuit neurons in the dentate gyrus of the rat hippocampus. Eur J Neurosci. 5:395–410.

Hefft S, Jonas P. 2005. Asynchronous GABA release generates long-lasting inhibition at a hippocampal interneuron-principal neuron synapse. Nat Neurosci. 8:1319–1328.

Hines ML, Carnevale NT. 1997. The NEURON simulation environment. Neural Comput. 9:1179–1209.

Hosp JA, Struber M, Yanagawa Y, Obata K, Vida I, Jonas P, Bartos M. 2014. Morpho-physiological criteria divide dentate gyrus interneurons into classes. Hippocampus. 24:189–203.

Jutras MJ, Fries P, Buffalo EA. 2009. Gamma-band synchronization in the macaque hippocampus and memory formation. J Neurosci. 29:12521–12531.

Karson MA, Tang AH, Milner TA, Alger BE. 2009. Synaptic cross talk between perisomatic-targeting interneuron classes expressing cholecystokinin and parvalbumin in hippocampus. J Neurosci. 29:4140–4154.

Kitchigina V, Popova I, Sinelnikova V, Malkov A, Astasheva E, Shubina L, Aliev R. 2013. Disturbances of septohippocampal theta oscillations in the epileptic brain: reasons and consequences. Exp Neurol. 247:314–327.

Klausberger T, Somogyi P. 2008. Neuronal diversity and temporal dynamics: the unity of hippocampal circuit operations. Science. 321:53–57.

Kobayashi M, Buckmaster PS. 2003. Reduced inhibition of dentate granule cells in a model of temporal lobe epilepsy. J Neurosci. 23:2440–2452.

Kraushaar U, Jonas P. 2000. Efficacy and stability of quantal GABA release at a hippocampal interneuron-principal neuron synapse. J Neurosci. 20:5594–5607.

Ma Y, Prince DA. 2012. Functional alterations in GABAergic fast-spiking interneurons in chronically injured epileptogenic neocortex. Neurobiol Dis. 47:102–113.

Magloczky Z, Toth K, Karlocai R, Nagy S, Eross L, Czirjak S, Vajda J, Rasonyi G, Kelemen A, Juhos V, et al. 2010. Dynamic changes of CB1-receptor expression in hippocampi of epileptic mice and humans. Epilepsia. 51(Suppl 3):115–120.

Morozov YM, Torii M, Rakic P. 2009. Origin, early commitment, migratory routes, and destination of cannabinoid type 1 receptor-containing interneurons. Cereb Cortex. 19(Suppl 1): i78–i89.

Mott DD, Turner DA, Okazaki MM, Lewis DV. 1997. Interneurons of the dentate-hilus border of the rat dentate gyrus: morphological and electrophysiological heterogeneity. J Neurosci. 17:3990–4005.

Obenaus A, Esclapez M, Houser CR. 1993. Loss of glutamate decarboxylase mRNA-containing neurons in the rat dentate gyrus following pilocarpine-induced seizures. J Neurosci. 13:4470–4485.

Peng Z, Zhang N, Wei W, Huang CS, Cetina Y, Otis TS, Houser CR. 2013. A reorganized GABAergic circuit in a model of epilepsy: evidence from optogenetic labeling and stimulation of somatostatin interneurons. J Neurosci. 33:14392–14405.

Pernia-Andrade AJ, Jonas P. 2014. Theta-gamma-modulated synaptic currents in hippocampal granule cells in vivo define a mechanism for network oscillations. Neuron. 81:140–152.

Proddutur A, Yu J, Elgammal FS, Santhakumar V. 2013. Seizure-induced alterations in fast-spiking basket cell GABA currents modulate frequency and coherence of gamma oscillation in network simulations. Chaos. 23:046109.

Rattka M, Brandt C, Loscher W. 2013. The intrahippocampal kainate model of temporal lobe epilepsy revisited: epileptogenesis, behavioral and cognitive alterations, pharmacological response, and hippoccampal damage in epileptic rats. Epilepsy Res. 103:135–152.

Rotstein HG, Pervouchine DD, Acker CD, Gillies MJ, White JA, Buhl EH, Whittington MA, Kopell N. 2005. Slow and fast inhibition and an H-current interact to create a theta rhythm in a model of CA1 interneuron network. J Neurophysiol. 94:1509–1518.

Santhakumar V, Aradi I, Soltesz I. 2005. Role of mossy fiber sprouting and mossy cell loss in hyperexcitability: a network model of the dentate gyrus incorporating cell types and axonal topography. J Neurophysiol. 93:437–453.

Savanthrapadian S, Meyer T, Elgueta C, Booker SA, Vida I, Bartos M. 2014. Synaptic properties of SOM- and CCK-expressing cells in dentate gyrus interneuron networks. J Neurosci. 34:8197–8209.

Shao LR, Dudek FE. 2005. Changes in mIPSCs and sIPSCs after kainate treatment: evidence for loss of inhibitory input to dentate granule cells and possible compensatory responses. J Neurophysiol. 94:952–960.

Sloviter RS, Ali-Akbarian L, Elliott RC, Bowery BJ, Bowery NG. 1999. Localization of GABA(B) (R1) receptors in the rat hippocampus by immunocytochemistry and high resolution autoradiography, with specific reference to its localization in identified hippocampal interneuron subpopulations. Neuropharmacology. 38:1707–1721.

Soriano E, Nitsch R, Frotscher M. 1990. Axo-axonic chandelier cells in the rat fascia dentata: Golgi-electron microscopy and immunocytochemical studies. J Comp Neurol. 293:1–25.

Sun C, Mtchedlishvili Z, Bertram EH, Erisir A, Kapur J. 2007. Selective loss of dentate hilar interneurons contributes to reduced synaptic inhibition of granule cells in an electrical stimulation-based animal model of temporal lobe epilepsy. J Comp Neurol. 500:876–893.

Sun C, Sun J, Erisir A, Kapur J. 2014. Loss of cholecystokinin-containing terminals in temporal lobe epilepsy. Neurobiol Dis. 62:44–55.

Thind KK, Yamawaki R, Phanwar I, Zhang G, Wen X, Buckmaster PS. 2010. Initial loss but later excess of GABAergic synapses with dentate granule cells in a rat model of temporal lobe epilepsy. J Comp Neurol. 518:647–667.

Tort AB, Komorowski R, Eichenbaum H, Kopell N. 2010. Measuring phase-amplitude coupling between neuronal oscillations of different frequencies. J Neurophysiol. 104:1195–1210.

Tort AB, Rotstein HG, Dugladze T, Gloveli T, Kopell NJ. 2007. On the formation of gamma-coherent cell assemblies by oriens lacunosum-moleculare interneurons in the hippocampus. Proc Natl Acad Sci USA. 104:13490–13495.

Vida I, Bartos M, Jonas P. 2006. Shunting inhibition improves robustness of gamma oscillations in hippocampal interneuron networks by homogenizing firing rates. Neuron. 49:107–117.

Wang XJ. 2010. Neurophysiological and computational principles of cortical rhythms in cognition. Physiol Rev. 90:1195–1268.

White JA, Banks MI, Pearce RA, Kopell NJ. 2000. Networks of interneurons with fast and slow gamma-aminobutyric acid type A (GABAA) kinetics provide substrate for mixed gamma-theta rhythm. Proc Natl Acad Sci USA. 97:8128–8133.

Whittington MA, Traub RD, Kopell N, Ermentrout B, Buhl EH. 2000. Inhibition-based rhythms: experimental and mathematical observations on network dynamics. Int J Psychophysiol. 38:315–336.

Worrell GA, Parish L, Cranstoun SD, Jonas R, Baltuch G, Litt B. 2004. High-frequency oscillations and seizure generation in neocortical epilepsy. Brain. 127:1496–1506.

Wu LG, Saggau P. 1995. GABAB receptor-mediated presynaptic inhibition in guinea-pig hippocampus is caused by reduction of presynaptic Ca2+ influx. J Physiol. 485(Pt 3):649–657.

Wulff P, Ponomarenko AA, Bartos M, Korotkova TM, Fuchs EC, Bahner F, Both M, Tort AB, Kopell NJ, Wisden W, et al. 2009. Hippocampal theta rhythm and its coupling with gamma oscillations require fast inhibition onto parvalbumin-positive interneurons. Proc Natl Acad Sci USA. 106:3561–3566.

Wyeth MS, Zhang N, Mody I, Houser CR. 2010. Selective reduction of cholecystokinin-positive basket cell innervation in a model of temporal lobe epilepsy. J Neurosci. 30:8993–9006.

Yu J, Proddutur A, Elgammal FS, Ito T, Santhakumar V. 2013. Status epilepticus enhances tonic GABA currents and depolarizes GABA reversal potential in dentate fast-spiking basket cells. J Neurophysiol. 109:1746–1763.

Yu J, Swietek B, Proddutur A, Santhakumar V. 2015. Dentate total molecular layer interneurons mediate cannabinoid-sensitive inhibition. Hippocampus. 25:884–889.

Zhang W, Buckmaster PS. 2009. Dysfunction of the dentate basket cell circuit in a rat model of temporal lobe epilepsy. J Neurosci. 29:7846–7856.

Zhang W, Yamawaki R, Wen X, Uhl J, Diaz J, Prince DA, Buckmaster PS. 2009. Surviving hilar somatostatin interneurons enlarge, sprout axons, and form new synapses with granule cells in a mouse model of temporal lobe epilepsy. J Neurosci. 29:14247–14256.

Zhou FW, Roper SN. 2014. Reduced chemical and electrical connections of fast-spiking interneurons in experimental cortical dysplasia. J Neurophysiol. 112:1277–1290.